iScience

CellPress

Article

Imidazopyridines as Potent KDM5 Demethylase Inhibitors Promoting Reprogramming Efficiency of Human iPSCs

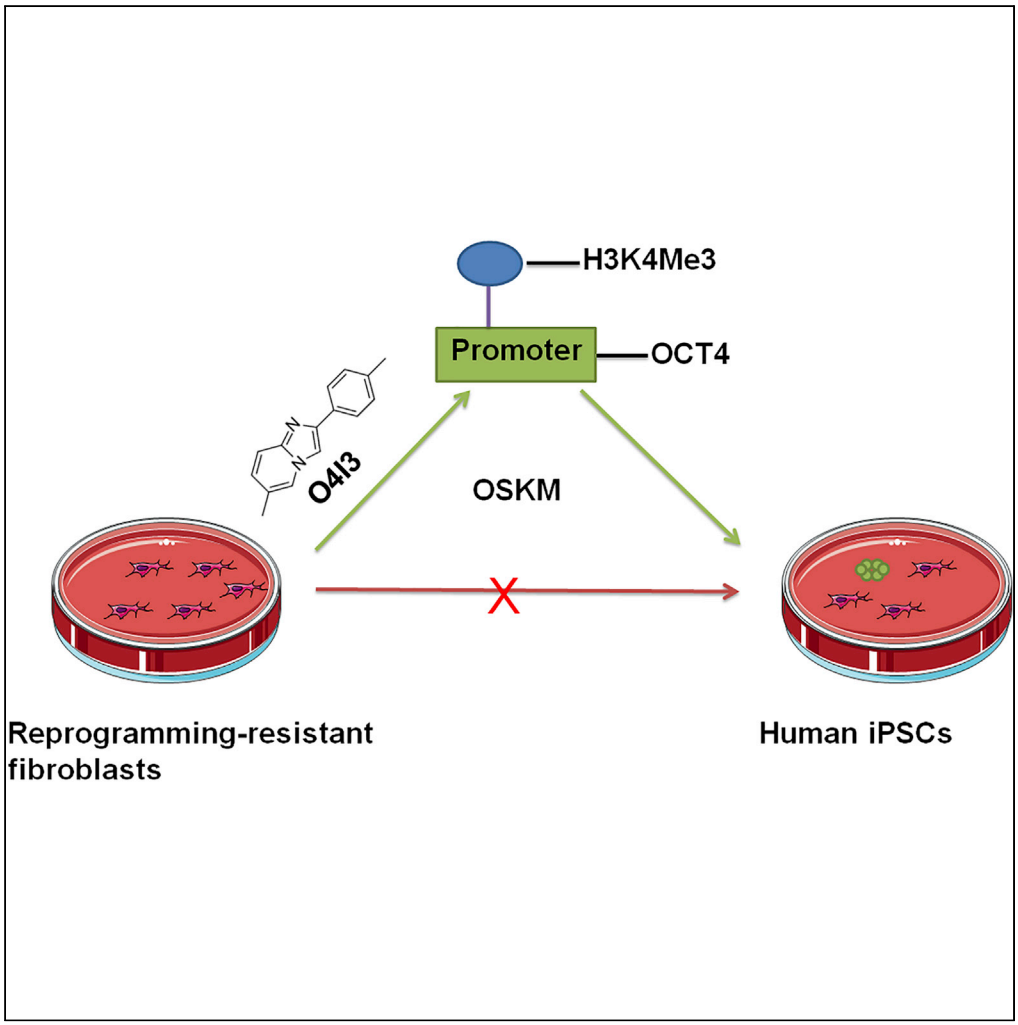

Yasamin Dabiri, Rodrigo A. Gama-Brambila, Katerina Taškova, ..., Jichang Wang, Miguel A. Andrade-Navarro, Xinlai Cheng

x.cheng@uni-heidelberg.de

HIGHLIGHTS

O4I3 supports the maintenance and generation of human iPSCs

O4I3 is a potent H3K4 demethylase KDM5 inhibitor *in vitro* and in cells

KDM5A, but not KDM5B, serves as an epigenetic barrier of reprogramming

Chemical or genetic inhibition of KDM5A tends to promote the reprogramming efficiency

Dabiri et al., iScience *12*, 168–181
February 22, 2019 © 2019 The Author(s).
https://doi.org/10.1016/j.isci.2019.01.012

iScience

CellPress

Article

Imidazopyridines as Potent KDM5 Demethylase Inhibitors Promoting Reprogramming Efficiency of Human iPSCs

Yasamin Dabiri,[1] Rodrigo A. Gama-Brambila,[1] Katerina Taškova,[2,3] Kristina Herold,[4] Stefanie Reuter,[4] James Adjaye,[5] Jochen Utikal,[6] Ralf Mrowka,[4] Jichang Wang,[7] Miguel A. Andrade-Navarro,[2,3] and Xinlai Cheng[1,8,*]

SUMMARY

Pioneering human induced pluripotent stem cell (iPSC)-based pre-clinical studies have raised safety concerns and pinpointed the need for safer and more efficient approaches to generate and maintain patient-specific iPSCs. One approach is searching for compounds that influence pluripotent stem cell reprogramming using functional screens of known drugs. Our high-throughput screening of drug-like hits showed that imidazopyridines—analogs of zolpidem, a sedative-hypnotic drug—are able to improve reprogramming efficiency and facilitate reprogramming of resistant human primary fibroblasts. The lead compound (O4I3) showed a remarkable OCT4 induction, which at least in part is due to the inhibition of H3K4 demethylase (KDM5, also known as JARID1). Experiments demonstrated that KDM5A, but not its homolog KDM5B, serves as a reprogramming barrier by interfering with the enrichment of H3K4Me3 at the OCT4 promoter. Thus our results introduce a new class of KDM5 chemical inhibitors and provide further insight into the pluripotency-related properties of KDM5 family members.

INTRODUCTION

Nuclear reprogramming from terminally differentiated somatic cells into induced pluripotent stem cells (iPSCs) is achieved by ectopic expression of several pluripotency-associated transcription factors, including OCT4, SOX2, KLF4, MYC, NANOG, or LIN28 (Takahashi et al., 2007; Takahashi and Yamanaka, 2006; Yu et al., 2007). This seminal technology provides a promising source for autologous organ transplantation, drug discovery, and disease modeling, opening a new era in the field of regenerative medicine (Smith et al., 2016; Takahashi and Yamanaka, 2016). When compared with somatic cell nuclear transfer, reprogramming of human fibroblasts (HFs) is a time-consuming (3–4 weeks) and inefficient (<0.01% of cells) process (Yamanaka and Blau, 2010). Somatic cell reprogramming can also be hampered by random mutations appearing in the course of reprogramming and during maintenance (Gore et al., 2011; Hussein et al., 2011; Ma et al., 2014). To reduce the risk of genetic and epigenetic variations in human iPSC (hiPSC), higher reprogramming efficiency and optimized cultivation conditions are of great importance. Furthermore, improved reprogramming efficiency for the generation of individual patient's own iPSCs will allow the development of personalized transplantation that avoids risks such as immune rejection caused by allogeneic transplantation (Morizane et al., 2013; Shiba et al., 2016). When compared with genetic manipulation, small molecules show advantages in controlling the reprogramming process and have been intensively investigated (Xie et al., 2017). Small molecules contribute to the establishment of more efficient and reliable protocols for the generation and maintenance of pluripotent stem cells (PSCs) (Watanabe et al., 2007). Although mouse chemically induced PSCs have been obtained by small-molecule cocktails (Hou et al., 2013), it seems that HFs are more resistant and chemical cocktails for generation of human iPSCs are not available yet.

A successful reprogramming process from fibroblasts to iPSCs requires proper histone modification, such as the repression of mesenchymal-associated markers and activation of pluripotency-associated genes (Mikkelsen et al., 2008). In general, hypermethylation of H3K4 is found close to transcription start sites (TSS) and is related to gene activation, whereas methylations of H3K27 and H3K9 represses gene expression (Papp and Plath, 2013). Very recently, analysis of the global landscape of histone markers confirmed the enrichment of H3K27Me3 and H3K9Me3, and the lack of H3K4Me3 at promoters of

[1]Institute of Pharmacy and Molecular Biotechnology, Heidelberg University, ImNeuenheimer Feld 364, 69120 Heidelberg, Germany

[2]Faculty of Biology, University Mainz, Gresemundweg 2, 55128 Mainz, Germany

[3]Institute of Molecular Biology GmbH, Ackermannweg 4, 55128 Mainz, Germany

[4]Experimentelle Nephrologie, KIM III, Universitätsklinikum, 07743 Jena, Germany

[5]Institute for Stem Cell Research and Regenerative Medicine, Heinrich Heine University, 40225 Düsseldorf, Germany

[6]Skin Cancer Unit, German Cancer Research Center (DKFZ) and Department of Dermatology, Venereology and Allergology, University Medical Center Mannheim, Ruprecht-Karl University of Heidelberg, 68167 Mannheim, Germany

[7]Center for Stem Cell Biology and Tissue Engineering, Key Laboratory for Stem Cells and Tissue Engineering, Ministry of Education, Department of Histology and Embryology, Zhongshan School of Medicine, Sun Yat-Sen University, Guangzhou 510275, China

[8]Lead Contact

*Correspondence: x.cheng@uni-heidelberg.de

https://doi.org/10.1016/j.isci.2019.01.012

 © 2019 The Author(s).
This is an open access article under the CC BY-NC-ND license (http://creativecommons.org/licenses/by-nc-nd/4.0/).

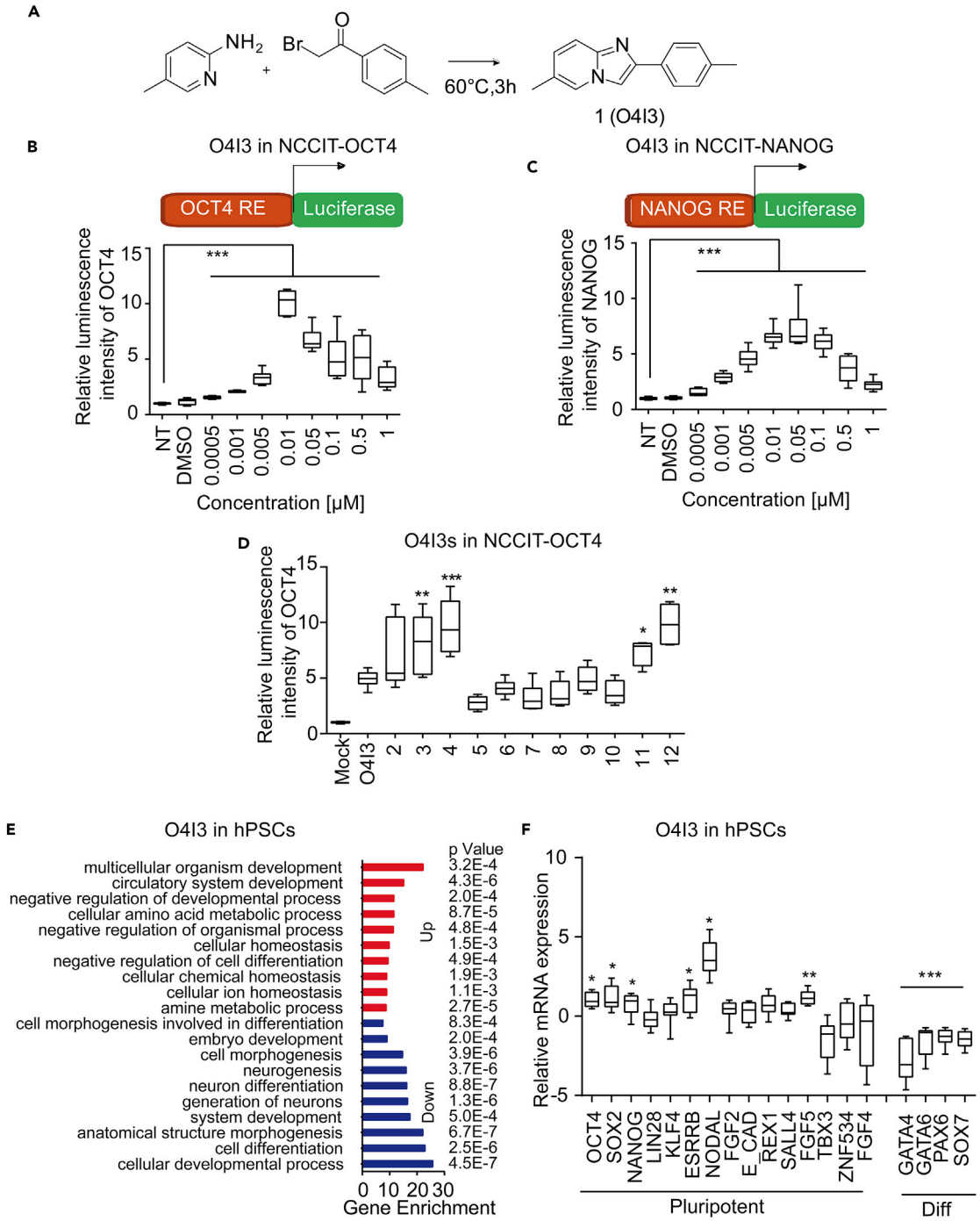

Figure 1. Identification of Imidazopyridine Analogs as OCT4-Inducing Compounds

(A) Synthesis of the compound 1.

(B and C) (B) O4I3 activates OCT4 in NCCIT-OCT4 response element (RE)-driven luciferase reporter cells and (C) NANOG in NCCIT-NANOG RE-driven luciferase reporter cells after 48h treatment.

(D) Activity of O4I3 derivatives (50 nM) in NCCIT-OCT4 cells.

(E) Functional enrichment analysis shows statistically significant enrichment in Gene Ontology terms related to pluripotency, development, and homeostasis in O4I3-treated PSCs for 24 h. Red, upregulated genes; blue, downregulated genes. p values represent values after multitest adjustment (see details in Transparent Methods).

Figure 1. *Continued*

(F) qRT-PCR analysis of pluripotency- and differentiation (diff)-related gene expression in O4I3-treated hPSCs at a concentration of 10 nM for 48 h.
In (B), (C), and (F) statistical significance was compared with mock (01% DMSO) treatment, whereas in (D) it was compared with O4I3 treatment using two-way ANOVA and a post-hoc Tukey test. Data are represented as mean ± SD. ***p<0.001, **p<0.01, *p<0.05.

reprogramming-associated genes in the reprogramming-resistant naked mole rat fibroblasts (Tan et al., 2017). To overwhelm epigenetic barriers, a number of chemical inhibitors targeting histone methyltransferases (HMTs), histone demethylases (HDMs), and histone deacetylase (HDAC) have been introduced for reprogramming (Xie et al., 2017). KDM5, also known as JARID1, is a H3K4-specific HDM and is considered as a repressor of gene expression (Kooistra and Helin, 2012). Little is known about the function of KDM5 chemical inhibitors in somatic cell reprogramming.

We report that 2-arylpyrimidazoles, including zolpidem, (a US Food and Drug Administration-approved drug for insomnia treatment; Weitzel et al., 2000) act as pluripotency inducers to promote the generation of iPSCs from patient fibroblasts by targeting H3K4-specific demethylase, KDM5. We show that KDM5A, but not its family member KDM5B, is an epigenetic barrier in somatic cell reprogramming.

RESULTS

Identification of Imidazopyridines as OCT4 Inducers by Cell-Based High-Throughput Screening

In an effort to find new chemical pluripotency inducers, we performed high-throughput screenings (HTSs) from a library containing ~250,000 chemicals. The screen was based on cellular luciferase reporter assays, controlled by the promoter activity of pluripotency-associated transcription factors in HEK293 cells (Cheng et al., 2015a, 2015b). Drug repurposing provides a successful way to develop new therapies with known, medically approved drugs within remarkably short periods (Cragg et al., 2014). With the expectation of having advantages in terms of pharmacodynamics and pharmacokinetics, we intentionally sought for chemicals sharing backbones with approved drugs. In the screen, we found nearly 4,000 imidazopyridine derivatives with significantly differential luciferase activities in the HEK-OCT4 reporter cell line (Figure S1A). To study this class of compounds in detail, we selected and synthesized the lead structure, 6-methyl-2-(p-tolyl)imidazo[1,2-a]pyridine (compound 1, Figure 1A), by heating ω-bromoacetophenone with an excess of 2-aminopyridine for 3 h to achieve a yield of >95% (Buu-Hoï et al., 1954).

To examine the activity of endogenous OCT4 and its downstream gene NANOG, we generated reporter cell lines in human embryonic carcinoma cell lines (NCCIT), whose luciferase transcription is driven by response elements of either OCT4 (NCCIT-OCT4) or NANOG (NCCIT-NANOG). We found nearly 10-fold inductions of both OCT4 and NANOG by compound 1 at low nanomolar doses when compared with untreated cells (Figures 1B, 1C, and S1B). We then referred to it as *OCT4-inducing compound 3* (O4I3). It has been shown that transient overexpression of OCT4 can lead to the differentiation of embryonic stem cells (ESCs) to extraembryonic endoderm and mesoderm (Niwa et al., 2000; Ovitt and Scholer, 1998). We found the induction of T and GATA4 in human PSCs (hPSCs) treated with 10 μM O4I3 (Figure S1C), suggesting that O4I3 might transiently hyperactivate OCT4 at high concentrations, which led to the differentiation and reduction of OCT4 activity (Figure 1B). We also tested the activity of zolpidem (containing the imidazopyridine backbone) in both reporter cell lines and detected an approximate 2-fold induction in NCCIT-OCT4 and NANOG reporter cells at a concentration of 10 μM (Figures S1D and S1E). Collectively, these results documented that O4I3 and zolpidem activated OCT4 at both the transcriptional and translational levels.

Pan-assay interference compounds are a class of compounds, referring to the hits from HTS, which give rise to an artificial signal in a drug-unlike manner (Baell and Walters, 2014). We chemically expanded O4I3 by replacing the CH_3 group at the phenyl moiety with various substituents on the aryl moiety (Table S1) and found that compounds induced drug-like, structure-dependent activations in NCCIT-OCT4 cells (Figure 1D).

O4I3 Maintains Pluripotency of Human iPSCs

Functional annotation and enrichment analysis of DNA microarray in O4I3-treated hPSCs showed that O4I3 (10 nM) promoted hPSC homeostasis and repressed cellular differentiation (Figures 1E and S2A). qRT-PCR results confirmed that O4I3 stabilized or slightly increased the expression of pluripotency-associated

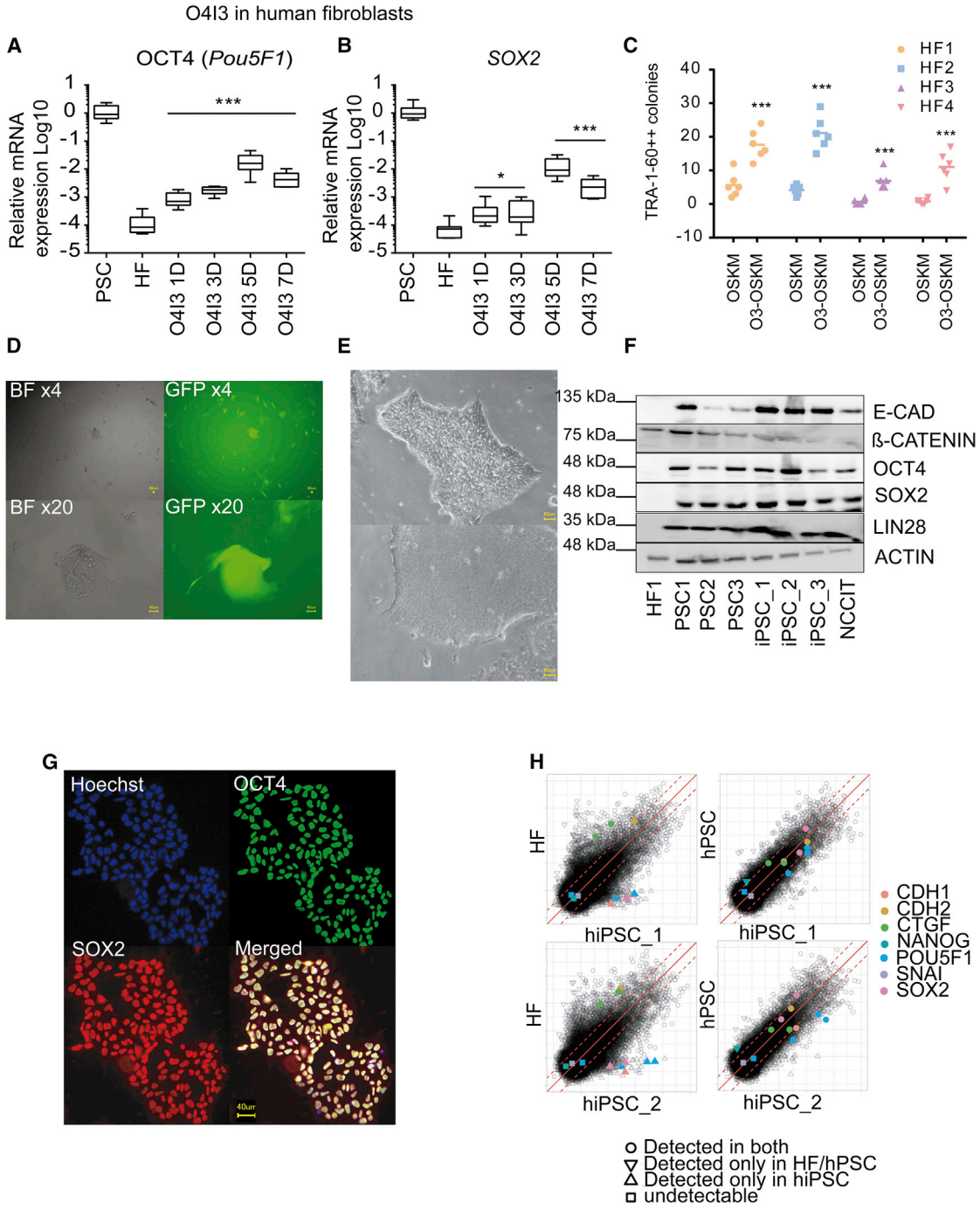

Figure 2. O4I3 Improves OSKM-Induced Reprogramming

(A and B) (A) O4I3 induces OCT4 and (B) SOX2 expression in human fibroblasts treated with O4I3 (50 nM) for the indicated time points (D, days).

(C) Efficiency of OSKM-induced reprogramming in the presence or absence of O4I3 in human fibroblasts 1–4 (HF1–HF4). ESC-like colonies were detected by TRA-1-60 staining.

(D) Reprogramming of resistant fibroblasts carrying LTR7-EGFP promoter. ESC-like GFP+ colonies were observed in bright field (BF) and GFP channel (GFP).

(E) ESC-like colonies detected from newly generated hiPSC lines.

(F) Expression of pluripotency-associated markers in the newly generated iPSC1, 2, and 3 when compared with hPSC1–3 as positive controls, determined by immunoblotting.

(G) Co-expression of OCT4 and SOX2 in the newly generated iPSCs.

Figure 2. *Continued*

(H) Scatterplots of gene expression data show high similarity between the newly generated iPSCs (hiPSC_1 and hiPSC_2) and hPSC (positive control), but not human fibroblasts (HF). All scatterplots are based on log2-transformed gene expression values. Red dashed lines depict the 2-fold change in expression values.

In (A) and (B) statistical significance was compared with mock (0.1% DMSO) treatment in fibroblasts, whereas in (C) it was compared with the efficiency obtained by ectopic expression of OSKM using two-way ANOVA followed by a post-hoc Tukey test. Data are represented as mean ± SD. ***p<0.001, **p<0.01, *p<0.05.

genes (OCT4, SOX2, NANOG, and NODAL) and suppressed differentiation-related gene expression (GATA4, GATA6, PAX6, and SOX7) (Figure 1F). Cellular viability of hPSCs was increased up to 4-fold at low nanomolar concentrations of O4I3 when compared with cells treated with Rock inhibitor (Y-27632) (Figure S2B), a small molecule able to increase hPSC survival (Watanabe et al., 2007). Fluorescence-activated cell sorting (FACS) analysis confirmed that O4I3 (10 nM) supports pluripotency during the maintenance of hPSCs after at least 30 passages under feeder-free conditions as shown by the expression of TRA-1-81 and OCT4 (Figure S2C). In addition, zolpidem also promoted the maintenance of iPSCs at a concentration of 10 μM (Figure S2B).

O4I3 Promotes the Conversion of Human Resistant Fibroblasts into hiPSCs

Analyzing the effects of O4I3 on HFs, we detected the activation of reprogramming-associated genes at the mRNA level (Figures 2A, 2B, and S3A), which included an approximately 10-fold induction of OCT4 (~0.1% versus in hPSCs) and NANOG (~1% versus hPSCs) and an about 100-fold increase of SOX2 (~1% versus hPSCs) and CDH1 (~10% versus hPSCs). We applied O4I3 in a commercially available episome-based reprogramming cocktail suitable for biosafety level 1 laboratory (Okita et al., 2011). These episomal vectors induce the expression of OCT4, SOX2, KLF4, LIN28, and L-MYC, and suppress p53 expression (referred to as OSKM). When compared with OSKM-only-treated fibroblasts, adding O4I3 (50 nM) to the cocktail increases the number of TRA-1-60-positive colonies (10–20 times) in both human primary fibroblasts (HF1 and HF2, Figure 2C).

Studies have reported that senescence and other unknown cellular processes can confer donor fibroblasts resistance to reprogramming (Hayashi et al., 2016; Shore et al., 2006; Yamanaka, 2009). We tested if O4I3 enables reprogramming of refractory fibroblasts. For this, the following two HF cell lines resistant to OSKM-mediated reprogramming were selected: (1) the HFF-LTR7-EGFP cell line (at passage >40), which expresses EGFP under the control of the LTR7 promoter, known to be activated during reprogramming (Wang et al., 2014), and (2) HF4, isolated from a patient sample (Figure 2C). iPSC-like colonies appeared in both cases in the presence of O4I3 (Figures 2C and 2D) as well as in the presence of zolpidem at a concentration of 10 μM (Figure S3B).

Characterization of the Newly Generated hiPSCs

We expanded hiPSC-like colonies and cultivated them for at least 30 passages under feeder-free conditions. Established hiPSC lines showed typical human ESC morphology (Figure 2E) and expressed pluripotency markers such as OCT4, SOX2, E-Cadherin, and NANOG in a comparable manner to those in hPSCs (Figures 2F and 2G). More than 95% of new hiPSCs co-expressed TRA-1-60 and E-Cadherin, as well as TRA-1-81 and OCT4 analyzed by FACS (Figure S3C). Comparative DNA microarray data showed that pluripotency-associated genes (Pou5F1 encoding OCT4, CDH1 encoding E-Cadherin, EPCAM, and DNMT3B) were highly expressed in hiPSC_1 and hiPSC_2, whereas fibroblast-related genes (CDH2, TWIST1, TWIST2, and SNAI2) were suppressed (Figure S4A). Visualization of global gene expression profiles by both scatterplots and heatmap shows a higher similarity of gene expression patterns between the newly generated hiPSCs and hPSCs (as positive controls) when compared with that of HF (Figures 2H and S4B). Moreover, differentiated hiPSCs showed expression of markers of mesoderm (T, SLUG, and SNAI1), ectoderm (PAX6, Nestin, and Tuj1), and endoderm (AFP, FOXA2, and SOX17) (Figures S4C and S4D) using respective standard protocols, which further confirmed the pluripotency properties of the new hiPSCs.

O4I3 Is an Epigenetic Modulator

To obtain further insight into the mechanism of action of O4I3, we compared the global gene expression of HF, HF treated with O4I3 (HF-O4I3), HF transfected with episomal OSKM (HF-OSKM), and hiPSCs. Overlap in over 40% of all regulated genes was observed among HF-O4I3, HF-OSKM, and hiPSCs (Figure 3A), including genes

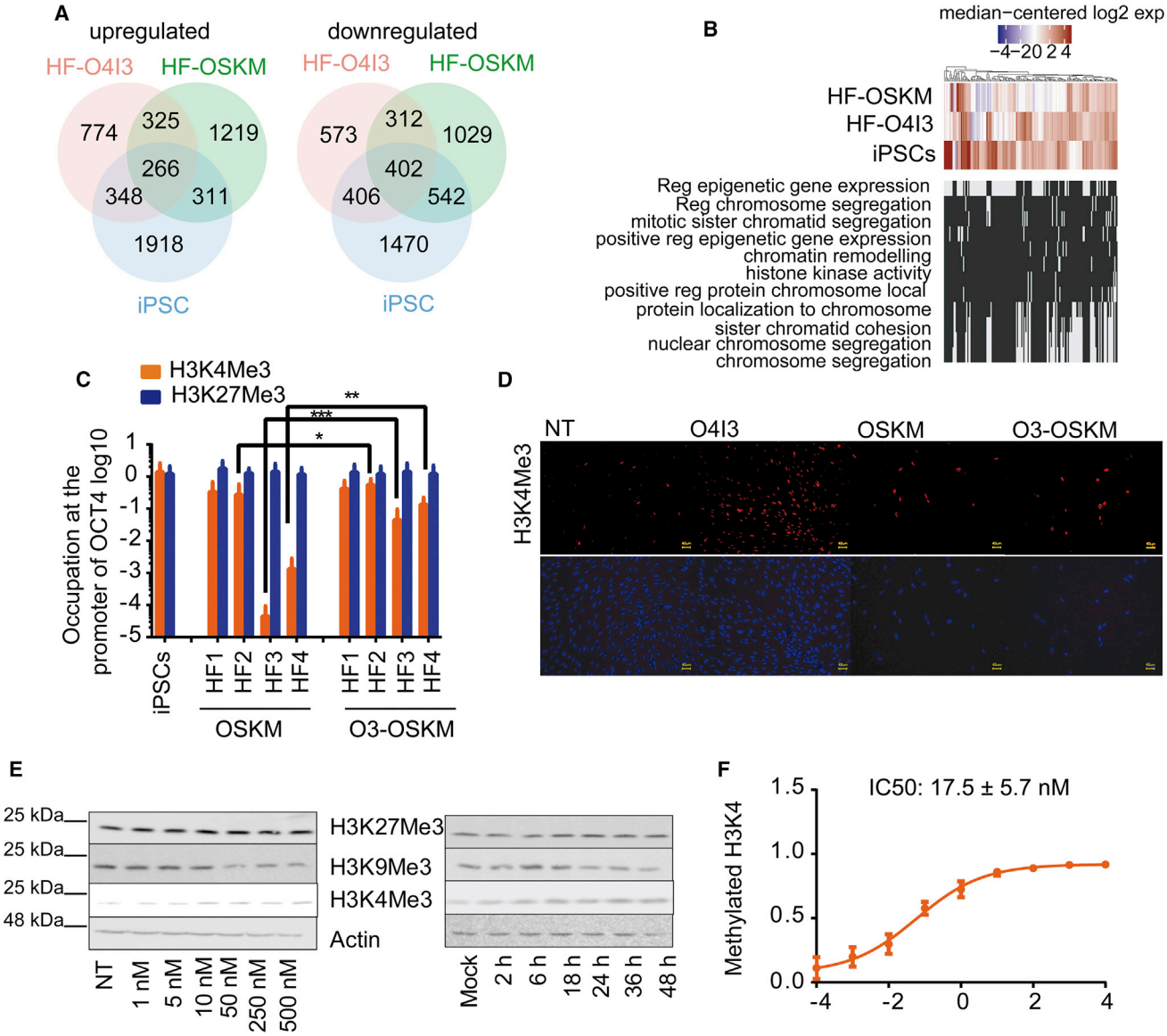

Figure 3. O4I3 Is an Epigenetic Modulator

(A) Venn diagram of up- and downregulated genes in O4I3 (50 nM)-treated human fibroblasts (HF) with ectopic expression of OCT4, SOX2, KLF4, and MYC (OSKM) as well as hiPSCs. HF-O4I3, HF cells treated with O4I3 (50 nM for 24 h); HF-OSKM, HF cells transfected with episomal OSKM; iPSCs, the newly generated iPSCs. Differential expression was calculated with respect to HF cells.

(B) Comparison of expression profiles of genes involved in epigenetic modification, chromatin remodeling, and related biological processes.

(C) Occupation of H3K4Me3 or H3K27Me3 at the promoter of OCT4 in HF cells transfected with OSKM alone or in the presence of 50 nM of O4I3 (O3-OSKM) for 3 days.

(D) O4I3 elevates the global levels of H3K4Me3 detected by immunocytochemistry. Cells were treated with 250 nM O4I3 for 3 days. Scale bar, 40 μm.

(E) Immunoblotting results show that O4I3 promotes global H3K4Me3 expression, whereas it represses H3K9Me3 protein levels in a concentration- and time-dependent manner. Cells were treated either with increasing concentrations of O4I3 for 24 h or with 250 nM of O4I3 for the indicated time points.

(F) O4I3 protects the methylation of H3K4, as observed by an *in vitro* methylation assay using total nuclear extraction.

In (C) statistical significance was compared with OSKM-treated fibroblasts using two-way ANOVA followed by a post-hoc Tukey test. Data are represented as mean ± SD. ***p<0.001, **p<0.01, *p<0.05.

involved in cell cycle progression and DNA replication (e.g., CDK1, MYC, and CDC25), and mesenchymal-epithelial-transition-associated genes (upregulation of CDH1 encoding E-Cadherin, EPCAM, CRB3, and OCLN, as well as downregulation of TWIST2). More than 30% of them were found to be involved in epigenetic

modification and chromatin remodeling (Figures 3B and S5A), for example, OCT4 (POU5F1), LIN28, MYCN, KIFs, DNMT3B, HDAC2, TET1, EZH2, and JARID2, which are of importance in somatic reprogramming and maintenance of pluripotency (Apostolou and Hochedlinger, 2013; Mikkelsen et al., 2008). We performed Gene Ontology (GO)-based functional enrichment analysis of regulated genes in HF-O4I3 compared with HF and found that a number of specialized terms associated with epigenetic and chromatin regulation were on top of the regulated terms (Figure 3B), including sister chromatid segregation (GO:0000819) and sister chromatid cohesion (GO:0007062), ribonucleoprotein complex biogenesis (GO:0022613), organelle fission (GO:0048285), and DNA replication (GO:0006260). Gene enrichment analysis on RNA sequencing also showed that the top signaling pathways regulated by O4I3 in HFs included regulation of organismal process, system development and embryo implantation, as well as cell differentiation (Figure S5A)

Recently, Onder and co-workers performed a loss-of-function screen of 22 epigenetic regulators and found that the inhibition of DOT1L and eight other genes promoted iPSC generation (Onder et al., 2012). We found that O4I3 significantly repressed six of these nine genes, including DOT1L (Figure S5B).

O4I3 Promotes the Methylation of H3K4

hiPSC derivation is an epigenetic reprogramming process (Xie et al., 2017). Genome-wide analysis of histone modification and chromatin remodeling revealed the number of alternations occurring at the early stage of reprogramming, including the hypermethylation of H3K4 (Koche et al., 2011) and the demethylation of H3K27 and H3K9 (Chen et al., 2013; Tan et al., 2017). These loosen the compacted heterochromatin and promote transcription factors binding to the "open" chromatin to initiate the reprogramming (Koche et al., 2011; Soufi et al., 2012).

We investigated the transfection efficiency in HF1 and HF4 using the same episomal vector carrying cytomegalovirus (CMV)-driven GFP (Okita et al., 2011). We could not observe a significant difference between two cell lines, as determined by FACS analysis (Figure S5C). This result suggested that the resistance was unlikely associated with low transfection efficiency. To study the epigenetic effects of O4I3 and its relevance to reprogramming, we focused on two histone modifications at the promoter of OCT4, namely, H3K4Me3, known to be related to gene activation, and H3K27Me3, which indicates gene repression. Chromatin immunoprecipitation-qPCR results in two reprogrammable fibroblasts (HF1 and HF2) and in two reprogramming-resistant fibroblasts (HF3 and HF4) showed that OSKM was sufficient to induce abundant occupation of H3K4Me3 at the promoter of OCT4 in HF1 and HF2 in a comparable manner to those in iPSCs, while producing 1,000- to 10,000-fold less in reprogramming-resistant cells (Figures 3C and S5D). The level of H3K27Me3 at the OCT4 promoter was minimally affected in our experiments (Figure 3C). Analysis on the global level of H3K4Me3 by immunocytochemistry showed the increase of H3K4Me3 upon O4I3 treatment (Figures 3D and S5E). Immunoblotting confirmed a dose- and time-dependent increase of global H3K4Me3 expression in fibroblast, whereas H3K27Me3 remained mostly unaffected (Figure 3E). In an *in vitro* methylation assay, O4I3 protected methylated H3K4 with an IC_{50} value of 20 nM (Figure 3F). Trimethylation of H3K9 has been reported to block reprogramming by recruiting heterochromatin protein 1 to form heterochromatin at the core of pluripotency loci (Chen et al., 2013), which interferes with the hypermethylation of H3K4 (Binda et al., 2010). Accordingly, we found the reduction of global H3K9Me3 posterior to H3K4Me3 activation (Figures 3E and S5F).

O4I3 Is a Potent KDM5 Inhibitor

HMT and HDM are two major classes of enzymes, contributing to the regulation of histone methylation. Lysine-specific demethylase 1 (LSD1) and histone lysine demethylase 5 (KDM5, also known as JARID1) majorly catalyze demethylation of H3K4 (Kooistra and Helin, 2012). A few KDM5 chemical inhibitors have been reported to inhibit demethylation of H3K4, leading to an increase of global methylated H3K4 in various cell types (Johansson et al., 2016; Vinogradova et al., 2016; Wang et al., 2013). We tested the inhibitory effect of O4I3 on LSD1 and KDM5. KDM4 (also known as JMJD2), the HDM of H3K9 and H3K36, was also included. We found that O4I3 inhibited KDM5 with IC_{50} values of 0.79 nM, whereas it inhibited KDM4 with a 500-fold less potency (IC_{50}: 249 nM). In the case of LSD1, we hardly detected the inhibitory effect of the molecule even at a concentration of 100 μM (Figure 4A).

In mammalian cells, the KDM5 family consists of four members, namely, KDM5A (known as JARID1A), KDM5B (known as JARID1B or PLU1), KDM5C (JARID1C), and KDM5D (JARID1D or SMCY) (Johansson et al., 2016). Selectivity was found for KDM5A with an IC_{50} value of 0.19 nM, whereas 20-, 40-, and

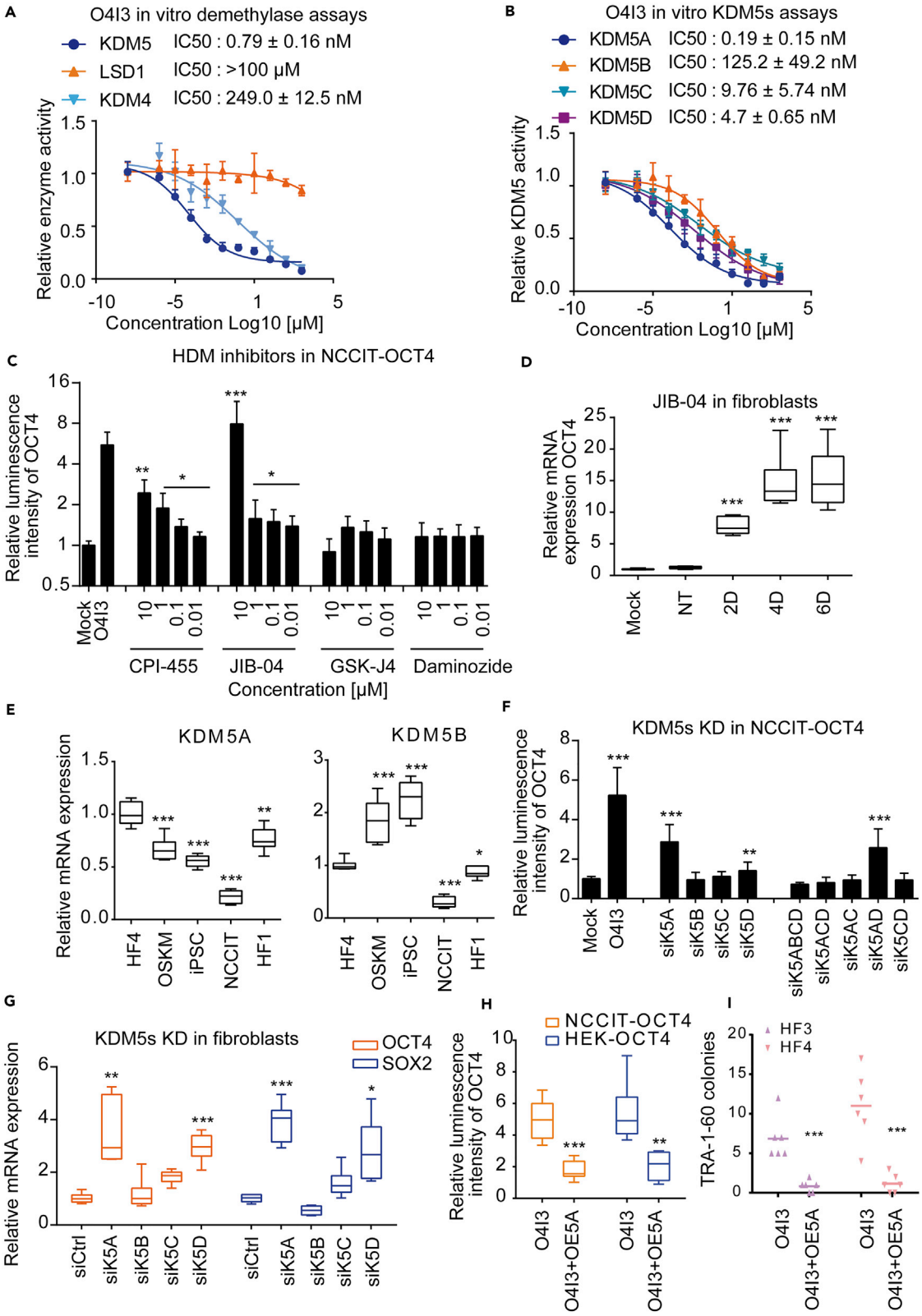
A
O4I3 in vitro demethylase assays
KDM5 IC50 : 0.79 ± 0.16 nM
LSD1 IC50 : >100 μM
KDM4 IC50 : 249.0 ± 12.5 nM
Relative enzyme activity
Concentration Log10 [μM]
B
O4I3 in vitro KDM5s assays
KDM5A IC50 : 0.19 ± 0.15 nM
KDM5B IC50 : 125.2 ± 49.2 nM
KDM5C IC50 : 9.76 ± 5.74 nM
KDM5D IC50 : 4.7 ± 0.65 nM
Relative KDM5 activity
Concentration Log10 [μM]
C
HDM inhibitors in NCCIT-OCT4
Relative luminescence intensity of OCT4
Mock
O4I3
CPI-455
JIB-04
GSK-J4
Daminozide
Concentration [μM]
D
JIB-04 in fibroblasts
Relative mRNA expression OCT4
Mock
NT
2D
4D
6D
E
KDM5A
KDM5B
Relative mRNA expression
HF4
OSKM
iPSC
NCCIT
HF1
F
KDM5s KD in NCCIT-OCT4
Relative luminescence intensity of OCT4
Mock
O4I3
siK5A
siK5B
siK5C
siK5D
siK5ABCD
siK5ACD
siK5AC
siK5AD
siK5CD
G
KDM5s KD in fibroblasts
OCT4
SOX2
Relative mRNA expression
siCtrl
siK5A
siK5B
siK5C
siK5D
H
NCCIT-OCT4
HEK-OCT4
Relative luminescence intensity of OCT4
O4I3
O4I3+OE5A
I
HF3
HF4
TRA-1-60 colonies
O4I3
O4I3+OE5A

Figure 4. O4I3 Is a Selective KDM5A Inhibitor

(A) Comparison of O4I3 inhibitory effect on KDM5, LSD1, and KDM4 *in vitro* using the whole-cell nuclear extraction.

(B) The inhibitory effect of O4I3 on the members of KDM5 family of demethylases isolated from cells.

(C) A selective KDM5A inhibitor JIB-04 induces OCT4 expression in NCCIT-OCT4 cells. Four histone demethylase inhibitors (HDMs), namely, CPI-455, JIB-04, GSK-J4, and daminozide, were incubated with NCCIT-OCT4 reporter cells for 48 h.

(D) JIB-04 (5 μM) induces OCT4 expression in fibroblasts at the indicated time points (D, days).

(E) Comparison of KDM5A and KDM5B expression levels in fibroblast (HF1), resistant fibroblast (HF4), HF4 transfected with OSKM, iPSCs, and NCCIT.

(F) Knockdown of KDM5A (si5A) activates OCT4 in NCCIT-OCT4 reporter cells. Cells were transfected with various KDM5 siRNA concentrations for 48 h.

(G) Transient knockdown (48 h) of KDM5A induces OCT4 and SOX2 expression in fibroblasts.

(H) Overexpression of KDM5A (OE5A) compromises the effect of O4I3 (100 nM, 48 h) in NCCIT-OCT4 and HEK-OCT4 cells.

(I) The number of TRA-1-60-positive colonies was reduced in reprogramming-resistant fibroblasts with overexpression of KDM5A.

In (C), (D), and (F) statistical significance was compared with mock (0.1% DMSO) treatment, in (G) with non-targeting siRNA and in (E) with HF4, whereas in (H) and (I) it was compared with OSKM-treated fibroblasts using two-way ANOVA followed by a post-hoc Tukey test. Data are represented as mean ± SD. ***$p<0.001$, **$p<0.01$, *$p<0.05$.

1,000-fold less potent IC_{50} values were obtained in the case of KDM5D, KDM5C, and KDM5B, respectively (Figure 4B). As expected, zolpidem protected H3K4 methylation and inhibited the expression of both KDM5 and KDM4 at micromolar concentrations (Figure S6A). Next, we tested four KDM chemical inhibitors. We found 3- and 5-fold induction of OCT4 expression in NCCIT-OCT4 reporter cell line in the presence of KDM5 inhibitors, CPI-455 (Vinogradova et al., 2016) and JIB-04 (Wang et al., 2013), respectively, but not in the presence of H3K27 demethylase inhibitor, GSK-J4 (Kruidenier et al., 2012) or the KDM2/7 inhibitor, daminozide (Rose et al., 2012), a plant growth regulator (Figure 4C). We detected the induction of OCT4, SOX2, and E-Cadherin expression in JIB-04-treated HFs (Figures 4D and S6B).

JIB-04 is a potent KDM5A inhibitor (IC_{50}: 230 nM) and was found to produce a higher induction of OCT4 compared with the pan KDM5 inhibitor, CPI-445 (Figure 4C). We questioned if the members of the KDM5 family contribute differently to the induction of pluripotency. KDM5B has been shown to be crucial in the early embryonic development and plays an important role in ESC maintenance (Xie et al., 2011) and neural differentiation (Schmitz et al., 2011). However, little is known about the function of other members of the KDM5 family of genes in development. We thus re-analyzed the KDM5A-D expression during human preimplantation (Vassena et al., 2011) and compared their expression patterns with those of the putative pluripotency markers, OCT4 and NANOG. KDM5B showed a similar expression pattern to OCT4 and NANOG, whereas KDM5A behaved oppositely (Figure S6C). In the case of KDM5D, the difference was not significant and KDM5C remained unaffected between ESC and oocyte (Figure S6C). We further compared the expression of KDM5A-5D in fibroblasts, reprogrammed fibroblasts by OSKM, iPSCs, and NCCIT (Figures 4E and S7A). KDM5A was preferentially expressed in reprogramming-resistant fibroblasts, whereas KDM5B was more pluripotency related (Figure 4E), which was in agreement with previous gene expression profiling data (Figure S7B) (Takahashi et al., 2014), as well as immunoblotting results (Figure S7C). As JIB-04 also inhibits KDM4 and KDM6 demethylases, we repressed the expression of KDM5A-D using RNA interference (small interfering RNA [siRNA]) and found significantly higher OCT4 reporter activity in NCCIT-OCT4 cells (Figure 4F), as well as higher mRNA levels of OCT4 and SOX2 in HFs in the absence of KDM5A and KDM5D expression, but not in KDM5B and KDM5C knockdown cells (Figures 4G and S7D). Notably, the effects of KDM5D repression were found to be less significant when compared with those of KDM5A knockdown, most probably due to the various transfection efficiencies (Figure S7D). Moreover, knockdown of KDM5A also increased the global levels of H3K4Me3 with or without OSKM (Figure S7E). Overexpression of KDM5A compromised these effects caused by KDM5A inhibition (either O4I3 or JIB-04) in NCCIT-OCT4 reporter cells in a concentration-dependent manner, as well as in HEK-OCT4 reporter cells (Figures 4H, S7F, and S7G). Conversely, cells were resistant to KDM5A chemical inhibitors in the absence of KDM5A expression (Figure S7G). Of note, at concentrations of 10 and 100 nM, O413 treatment alone showed higher OCT4 levels when compared with that of O4I3 combined with siRNA-mediated KDM5A inhibition (Figure S7G), which may be due to the insufficient knockdown efficiency (Figure S7D). As expected, overexpression of KDM5A also affected the formation of TRA-1-60-positive colonies in OSKM-mediated reprogramming of HFs (Figure 4I). Taken together, our results confirm the importance of KDM5A in the induction of pluripotency markers and the process of reprogramming of HFs.

Inhibition of KDM5A Promotes Reprogramming of Resistant Fibroblasts

In reprogramming-resistant HF4, the level of H3K4Me3 at the promoter of OCT4 was increased by OSKM, but was still nearly 1,000-fold lower than that in PSCs (Figure 5A). In combination with OSKM

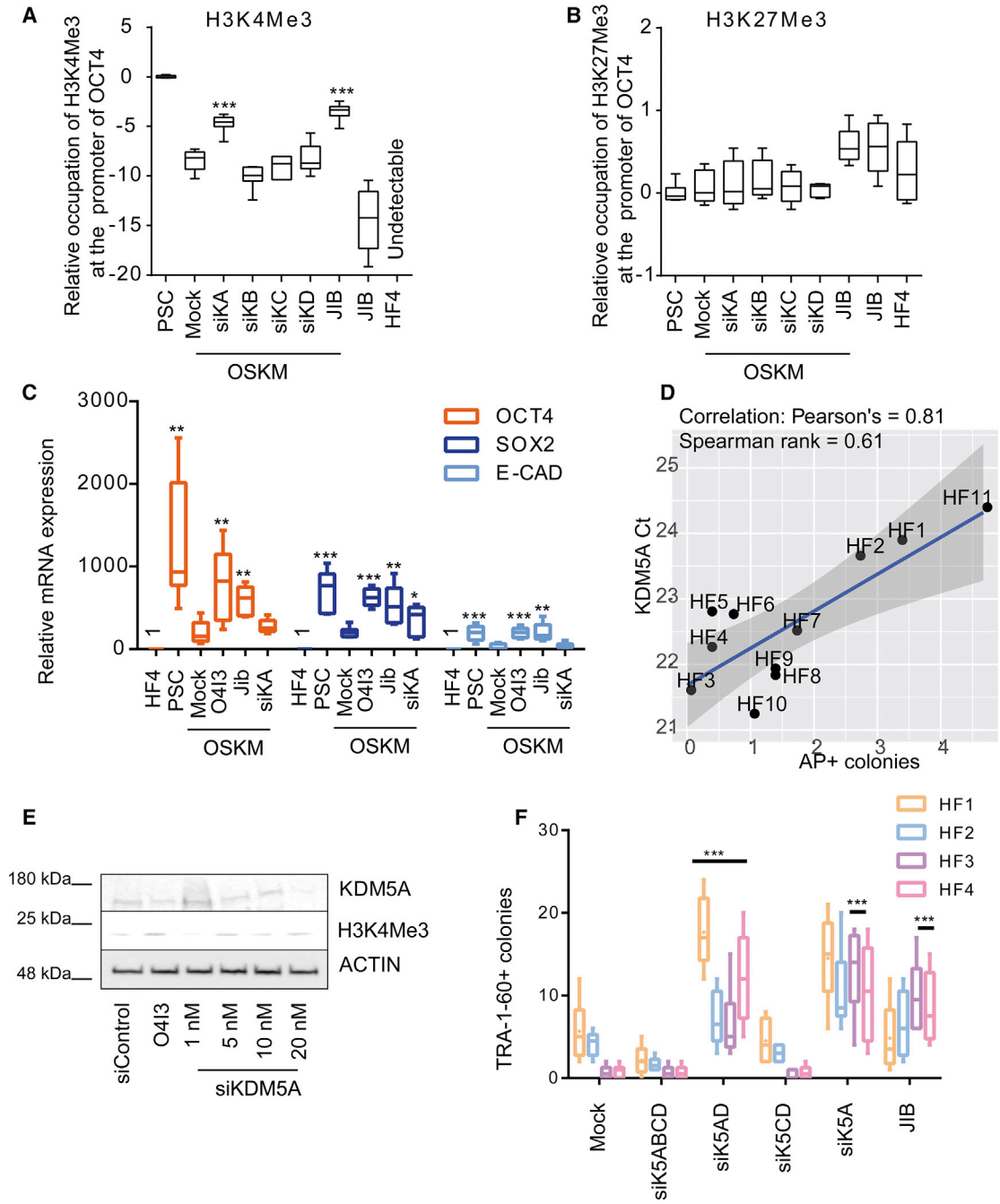

Figure 5. KDM5A Is a Reprogramming Barrier

(A and B) (A) Suppression of KDM5A activity by siRNA or JIB-04 (5 μM, 48 h) promotes the enrichment of H3K4Me3 at the promoter of OCT4 in resistant fibroblasts, (B) but not that of H3K27Me3. Ct values were obtained from qRT-PCR.

(C) Suppression of KDM5A activity by JIB-04 or KDM5A siRNA (siKA) induces POU5F1, SOX2, and CDH1 mRNA levels during reprogramming, as determined by qRT-PCR.

(D) Correlation between reprogramming efficiency and KDM5A expression in HF1-HF11. The same amount of each cDNA was used as template for qRT-PCR where the Ct values indicate the expression of KDM5A.

(E) Knockdown effects of increasing concentrations of anti-KDM5A siRNA (siKDM5A, 48 h) on H3K4Me3 expression levels in HF.

(F) Reprogramming efficiency using various patient primary fibroblasts, as determined by the number of TRA-1-60-positive colonies. Cells were either transiently transfected with the indicated siRNA oligos in the first 5 days or treated with JIB-04 (5 μM, 48 h). siK5ABCD, anti-KDM5A/B/C/D siRNA; siK5AD, anti-KDM5A/D siRNA; siK5CD, anti-KDM5C/D siRNA; siK5A, anti-KDM5A siRNA; siK5B, anti-KDM5B siRNA; siK5C, anti-KDM5C siRNA; and siK5D, anti-KDM5D siRNA. In (A), (B), and (F) statistical significance was compared with OSKM-treated fibroblasts, whereas in (C) it was compared with DMSO (0.1%) treatment using two-way ANOVA and a post-hoc Tukey test. Data are represented as mean ± SD. ***p<0.001, **p<0.01, *p<0.05.

overexpression, genetic repression of KDM5A expression using either KDM5A siRNA or chemical inhibition of KDM5A activity by JIB-04, significantly elevated the levels of H3K4Me3 (Figure 5A). However, a clear influence on H3K4 methylation was not observed in the presence of KDM5B-, KDM5C-, or KDM5D-siRNA (Figure 5A). Correspondingly, OSKM failed to force the expression of reprogramming-associated genes (POU5F1, SOX2, and CDH1) in the absence of KDM5A siRNA or JIB-04 in reprogramming-resistant fibroblasts (Figure 5C), implicating that OSKM was not sufficient to activate OCT4 to initiate reprogramming in those patient primary fibroblasts. Indeed, the reprogramming efficiency is negatively correlated with the expression of KDM5A in 11 HFs (Figure 5D). Moreover, KDM5A siRNA increased the global level of H3K4Me3 in a dose-dependent manner (Figures 5E and S7E). Of note, the alternation in the occupation of H3K27Me3 at the promoter of OCT4 was more refractory to chemical inhibition or genetic repression of KDM5s in our experiments (Figure 5B).

Transient suppression of KDM5A expression with either KDM5A siRNA or chemical inhibition mimicked the effect of O4I3 to either increase the episomal-based reprogramming efficiency in normal fibroblasts or to facilitate the formation of ESC-like TRA-1-60-positive colonies in reprogramming-resistant fibroblasts (Figures 5F and S8A). These ESC-like colonies could be isolated and expanded to establish stable hiPSC cell lines with the expression of pluripotency markers, like OCT4, SOX2, E-Cadherin, TRA-1-60, and TRA-1-81, and full differentiation potential (Figures S8B and S8C).

DISCUSSION

In 2006, Yamanaka and his co-workers successfully converted mouse fibroblasts into iPSCs with viral overexpression of OSKM (Takahashi and Yamanaka, 2006). This technology provides a simple approach to manipulate cell fate and thereby greatly advances the research in the field of regenerative medicine (Takahashi et al., 2007; Takahashi and Yamanaka, 2016). After a decade of research, the molecular mechanisms by which OSKM mediated somatic cell reprogramming are still incompletely understood. Reprogramming is a stochastic and inefficient process (Yamanaka, 2009). Initially, Takahashi et al. reported a reprogramming efficiency of 0.01% in HFs using retroviral infection (Takahashi et al., 2007). Recently, non-integrating reprogramming methods have been established, including episomal transfection, one of a few approaches suitable for biosafety level 1 laboratory. However, there are several shortcomings being associated with this technique, including low reprogramming efficiency (0.01%) (Schlaeger et al., 2015). Seeking for small molecules able to promote somatic cell reprogramming, we screened ~250,000 chemicals in cell-based assays and identified a series of O4Is (Cheng et al., 2015a, 2015b). Here, we report that O4I3, a compound sharing an imidazopyridine backbone with the anti-insomnia drug zolpidem (Weitzel et al., 2000), not only promotes the viability of hPSC in single-cell expansion and elevates the episome-based reprogramming efficiency (from ~0.01% to ~0.1%) but also importantly facilitates the reprogramming of patient primary fibroblasts, which are resistant to reprogramming.

In general, the ability of transcription factors to bind their corresponding promoter elements is influenced by epigenetic properties of the chromatin structure, including DNA methylation, histone modifications, and ATP-dependent chromatin remodeling. A number of studies have shown that Yamanaka transcription factors recruit a number of epigenetic modifiers including histone post-translational-modifying enzymes, nucleosome remodeling factors, and DNA methylation enzymes at multiple stages of the reprogramming process (Smith et al., 2016; Soufi et al., 2012). In terminally differentiated somatic cells, genomic DNA related to pluripotency is tightly compacted into nucleosomes, the basic structure of chromatin consisting of the histone octamer (two copies, each consists of four histone molecules) wrapped with a length of 146-base pair DNA, to form higher-order chromatin structures, called heterochromatin, for gene silencing (Papp and Plath, 2013). At the initial stage of reprogramming, the pioneer factors, OCT4, SOX2, and KLF4 (OSK), bind to the nucleosomal pluripotency loci preferentially at regions far from the TSS (TSS-distal), and also at TSS-proximal, and induce H3K4 methylation first at the enhancer regions 50–500 kb from TSS (Soufi et al., 2012, 2015) and later on at the promoters, resulting in gene expression changes (Atlasi and Stunnenberg, 2017; Soufi et al., 2015). Nevertheless, the influence of OSK on the pre-existing histone modifications, H3K27Me3, for instance, is very limited (Soufi et al., 2015). Furthermore, a genome-wide methylome analysis has previously revealed the gain of H3K4Me3 at promoters of pluripotency-associated genes during somatic cell reprogramming of mouse fibroblasts and B lymphocytes (Mikkelsen et al., 2008). Thus it is conceivable that applying chemicals that protect H3K4 methylation could overcome this epigenetic barrier during the reprogramming process. O4I3 not only enhanced the expression of global H3K4Me3 in cells and prevented the demethylation of H3K4 *in vitro* but also increased the occupancy of H3K4Me3 at the

promoter of OCT4. Consequently, exogenous reprogramming factors bind to promoter regions marked by trimethylated H3K4, which makes the chromatin structure more accessible.

Histone methylation is a reversible process. In mammals, the COMPASS (complex proteins-associated with SET1)-like proteins belong to the "writers" of H3K4, whereas KDM5s specifically remove ("erase") methyl groups from H3K4, unlike LSD1, which also demethylates H3K9Me1/2/3 (Kooistra and Helin, 2012). In this regard, the LSD1 inhibitor, parnate has been reported to promote reprogramming (Hou et al., 2013; Xie et al., 2017). Methylation of H3K9 represses gene expression and is considered as an epigenetic barrier for reprogramming (Chen et al., 2013). Thus parnate-induced pluripotency may be due to blocking the expression of differentiation-related genes via inhibition of H3K9 demethylation along with the activation of pluripotency markers through the enrichment of methylated H3K4 at their corresponding promoters or enhancers. We observed that O4I3 and zolpidem specifically inhibited KDM5 activity, an effect that could not be detected in the case of LSD1, suggesting that facilitation of H3K4 methylation at the promoter and enhancer regions of pluripotency genes might be the major reason for imidazopyridine-induced reprogramming in resistant fibroblasts.

Dynamic regulation of H3K4 methylation from oocyte stage to preimplantation suggests that KDM5s contribute to the embryonic development (Atlasi and Stunnenberg, 2017). Indeed, the essential role of KDM5B in ESC self-renewal and pluripotency has been reported (Schmitz et al., 2011; Xie et al., 2011). Re-analysis of gene expression data during human preimplantation (Vassena et al., 2011) interestingly showed a negatively correlated expression pattern of KDM5A when compared with that of KDM5B and to those of pluripotency markers, OCT4 and NANOG. We found that KDM5A was highly expressed in HFs and was repressed during cellular reprogramming. Thus the observation that O4I3 supported the maintenance and acquisition of pluripotency in HFs might be due to its selective inhibition on KDM5A. As a proof of concept, suppression of KDM5A expression either chemically, using the specific chemical inhibitor JIB-04 (Wang et al., 2013), or with siRNA mimicked the function of O4I3, in terms of induction of pluripotency markers, whereas ectopic expression of KDM5A compromised the effect of O4I3 on reprogramming. Recently, Pfaff et al. reported that de-repression of Kdm5A by miRNA-212/132 improved the reprogramming efficiency in murine embryonic fibroblasts (Pfaff et al., 2017). Mouse iPSCs are close to naive ESCs, whereas hiPSCs are rather primed pluripotent. Thus, it is interesting to investigate whether KDM5A plays opposing roles in naive and primed states of pluripotency.

The generation of patient-specific clinic-grade iPSCs is a prerequisite for applying transcription-factor-mediated reprogramming for personalized therapies. Compelling experimental results showed that the initiation of reprogramming is associated with hypermethylation of H3K4 at the promoters or enhancers of pluripotency genes. We identified a novel class of imidazopyridines as potent H3K4-specific KDM5 inhibitors through HTS and demonstrated that KDM5A, but not KDM5B, is an epigenetic barrier to reprogramming and that inhibition of KDM5A activity enables the induction of pluripotency in reprogramming-resistant patient-derived primary fibroblasts.

Limitations of the Study

There are several issues remaining to be addressed with regard to the inhibitory effect of O4I3 on KDM5 and its correlation with the induction of pluripotency, including (1) the influence of O413 on epigenetic modifiers other than those of the KDM5 family, such as other histone methyl transferases or demethylases; (2) the mode of interaction of O413 with KDM5 demethylase enzymes; and most importantly (3) the combinations of small molecules by which exogenous OCT4 can be replaced in the context of OSKM-mediated reprogramming.

METHODS

All methods can be found in the accompanying Transparent Methods supplemental file.

DATA AND SOFTWARE AVAILIBILITY

All DNA microarray data have been deposited in GEO under the accession number: GSE123668. RNA sequencing data have been deposited in the Bioproject database, NCBI. The accession number is SUB4899089.

SUPPLEMENTAL INFORMATION

Supplemental Information includes Transparent Methods, eight figures, and three tables and can be found with this article online at https://doi.org/10.1016/j.isci.2019.01.012.

ACKNOWLEDGMENTS

We thank Prof. Stefan Wölfl for his kind support and valuable suggestions. We thank Luuk N. van Oosten for his critical comments to the manuscript. We thank Jie Cheng for designing chemical synthesis and Sawsan Saleh and Felix Braun for helping with chemical synthesis and characterization. We thank Mohamed A. Abu el Maaty for performing protein ELISA microarray analysis. We thank Viola Mayer for her technical support. We thank Maryam Dabiri for her support in the preparation of the cover image.

This work is supported by the Bundesministerium für Bildung und Forschung (BMBF) grant programs Drug-iPS (FKZ 0315398A and B) and SysToxChip (FKZ 031A303A and E). X.C. is a recipient of the Deutsche Forschungsgemeinschaft (DFG) grant program (CH 1690/2-1), and Y.D. is a recipient of the "Landesgraduiertenförderung (LGF) fellowship program for individual doctoral training" from Universität Heidelberg.

AUTHOR CONTRIBUTIONS

Y.D. and R.A.G.-B. performed bioassessments. K.T. performed gene expression analyses as well as downstream data analyses. K.H., S.R., J.A., and R.M. established the reporter cell lines. J.U. isolated patient fibroblasts. J.W. performed RNA-seq experiment and data analysis. M.A.A.-N. was involved in the supervision of the bioinformatics analyses, manuscript correction, and discussion. X.C. designed and performed chemical syntheses as well as biological experiments, analyzed the data, and wrote the manuscript. All authors read and approved the manuscript before submission.

DECLARATION OF INTERESTS

J.A., R.M., and X.C. together with Heidelberg University hold a patent for O4I3 (EP: U21-16ERF).

Received: September 21, 2018
Revised: December 11, 2018
Accepted: January 8, 2019
Published: February 22, 2019

REFERENCES

Apostolou, E., and Hochedlinger, K. (2013). Chromatin dynamics during cellular reprogramming. Nature *502*, 462–471.

Atlasi, Y., and Stunnenberg, H.G. (2017). The interplay of epigenetic marks during stem cell differentiation and development. Nat. Rev. Genet. *18*, 643–658.

Baell, J., and Walters, M.A. (2014). Chemical con artists foil drug discovery. Nature *513*, 481–483.

Binda, O., LeRoy, G., Bua, D.J., Garcia, B.A., Gozani, O., and Richard, S. (2010). Trimethylation of histone H3 lysine 4 impairs methylation of histone H3 lysine 9: regulation of lysine methyltransferases by physical interaction with their substrates. Epigenetics *5*, 767–775.

Buu-Hoï, N.P., Jacquignon, P., Xuong, N.D., and Lavit, D. (1954). 2-ARYLPYRROLINES AND 2-ARYLPYRIMIDAZOLES. J. Org. Chem. *19*, 1370–1375.

Chen, J., Liu, H., Liu, J., Qi, J., Wei, B., Yang, J., Liang, H., Chen, Y., Chen, J., Wu, Y., et al. (2013). H3K9 methylation is a barrier during somatic cell reprogramming into iPSCs. Nat. Genet. *45*, 34–42.

Cheng, X., Dimou, E., Alborzinia, H., Wenke, F., Gohring, A., Reuter, S., Mah, N., Fuchs, H., Andrade-Navarro, M.A., Adjaye, J., et al. (2015a). Identification of 2-[4-[(4-Methoxyphenyl) methoxy]-phenyl]acetonitrile and derivatives as potent Oct3/4 inducers. J. Med.Chem. *58*, 4976–4983.

Cheng, X., Yoshida, H., Raoofi, D., Saleh, S., Alborzinia, H., Wenke, F., Gohring, A., Reuter, S., Mah, N., Fuchs, H., et al. (2015b). Ethyl 2-((4-Chlorophenyl)amino)thiazole-4-carboxylate and derivatives are potent inducers of Oct3/4. J. Med.Chem. *58*, 5742–5750.

Cragg, G.M., Grothaus, P.G., and Newman, D.J. (2014). New horizons for old drugs and drug leads. J. Nat. Prod. *77*, 703–723.

Gore, A., Li, Z., Fung, H.L., Young, J.E., Agarwal, S., Antosiewicz-Bourget, J., Canto, I., Giorgetti, A., Israel, M.A., Kiskinis, E., et al. (2011). Somatic coding mutations in human induced pluripotent stem cells. Nature *471*, 63–67.

Hayashi, Y., Hsiao, E.C., Sami, S., Lancero, M., Schlieve, C.R., Nguyen, T., Yano, K., Nagahashi, A., Ikeya, M., Matsumoto, Y., et al. (2016). BMP-SMAD-ID promotes reprogramming to pluripotency by inhibiting p16/INK4A-dependent senescence. Proc.Natl.Acad.Sci. U S A *113*, 13057–13062.

Hou, P.P., Li, Y.Q., Zhang, X., Liu, C., Guan, J.Y., Li, H.G., Zhao, T., Ye, J.Q., Yang, W.F., Liu, K., et al. (2013). Pluripotent stem cells induced from mouse somatic cells by small-molecule compounds. Science *341*, 651–654.

Hussein, S.M., Batada, N.N., Vuoristo, S., Ching, R.W., Autio, R., Narva, E., Ng, S., Sourour, M., Hamalainen, R., Olsson, C., et al. (2011). Copy number variation and selection during reprogramming to pluripotency. Nature *471*, 58–U67.

Johansson, C., Velupillai, S., Tumber, A., Szykowska, A., Hookway, E.S., Nowak, R.P., Strain-Damerell, C., Gileadi, C., Philpott, M., Burgess-Brown, N., et al. (2016). Structural analysis of human KDM5B guides histone demethylase inhibitor development. Nat. Chem. Biol. *12*, 539–545.

Koche, R.P., Smith, Z.D., Adli, M., Gu, H., Ku, M., Gnirke, A., Bernstein, B.E., and Meissner, A. (2011). Reprogramming factor expression initiates widespread targeted chromatin remodeling. Cell Stem Cell *8*, 96–105.

Kooistra, S.M., and Helin, K. (2012). Molecular mechanisms and potential functions of histone demethylases. Nature Rev. Mol. Cell Biol. *13*, 297–311.

Kruidenier, L., Chung, C.W., Cheng, Z., Liddle, J., Che, K., Joberty, G., Bantscheff, M., Bountra, C., Bridges, A., Diallo, H., et al. (2012). A selective jumonji H3K27 demethylase inhibitor modulates the proinflammatory macrophage response. Nature *488*, 404–408.

Ma, H., Morey, R., O'Neil, R.C., He, Y., Daughtry, B., Schultz, M.D., Hariharan, M., Nery, J.R., Castanon, R., Sabatini, K., et al. (2014). Abnormalities in human pluripotent cells due to reprogramming mechanisms. Nature *511*, 177–183.

Mikkelsen, T.S., Hanna, J., Zhang, X., Ku, M., Wernig, M., Schorderet, P., Bernstein, B.E., Jaenisch, R., Lander, E.S., and Meissner, A. (2008). Dissecting direct reprogramming through integrative genomic analysis. Nature *454*, 49–55.

Morizane, A., Doi, D., Kikuchi, T., Okita, K., Hotta, A., Kawasaki, T., Hayashi, T., Onoe, H., Shiina, T., Yamanaka, S., et al. (2013). Direct comparison of autologous and allogeneic transplantation of iPSC-derived neural cells in the brain of a non-human primate. Stem Cell Rep. *1*, 283–292.

Niwa, H., Miyazaki, J., and Smith, A.G. (2000). Quantitative expression of Oct-3/4 defines differentiation, dedifferentiation or self-renewal of ES cells. Nat. Genet. *24*, 372–376.

Okita, K., Matsumura, Y., Sato, Y., Okada, A., Morizane, A., Okamoto, S., Hong, H., Nakagawa, M., Tanabe, K., Tezuka, K., et al. (2011). A more efficient method to generate integration-free human iPS cells. Nat. Methods *8*, 409–412.

Onder, T.T., Kara, N., Cherry, A., Sinha, A.U., Zhu, N., Bernt, K.M., Cahan, P., Marcarci, B.O., Unternaehrer, J., Gupta, P.B., et al. (2012). Chromatin-modifying enzymes as modulators of reprogramming. Nature *483*, 598–602.

Ovitt, C.E., and Scholer, H.R. (1998). The molecular biology of Oct-4 in the early mouse embryo. Mol. Hum.Reprod. *4*, 1021–1031.

Papp, B., and Plath, K. (2013). Epigenetics of reprogramming to induced pluripotency. Cell *152*, 1324–1343.

Pfaff, N., Liebhaber, S., Mobus, S., Beh-Pajooh, A., Fiedler, J., Pfanne, A., Schambach, A., Thum, T., Cantz, T., and Moritz, T. (2017). Inhibition of miRNA-212/132 improves the reprogramming of fibroblasts into induced pluripotent stem cells by de-repressing important epigenetic remodelling factors. Stem Cell Res. *20*, 70–75.

Rose, N.R., Woon, E.C., Tumber, A., Walport, L.J., Chowdhury, R., Li, X.S., King, O.N., Lejeune, C., Ng, S.S., Krojer, T., et al. (2012). Plant growth regulator daminozide is a selective inhibitor of human KDM2/7 histone demethylases. J. Med.Chem. *55*, 6639–6643.

Schlaeger, T.M., Daheron, L., Brickler, T.R., Entwisle, S., Chan, K., Cianci, A., DeVine, A., Ettenger, A., Fitzgerald, K., Godfrey, M., et al. (2015). A comparison of non-integrating reprogramming methods. Nat.Biotechnol. *33*, 58–63.

Schmitz, S.U., Albert, M., Malatesta, M., Morey, L., Johansen, J.V., Bak, M., Tommerup, N., Abarrategui, I., and Helin, K. (2011). Jarid1b targets genes regulating development and is involved in neural differentiation. EMBO J. *30*, 4586–4600.

Shiba, Y., Gomibuchi, T., Seto, T., Wada, Y., Ichimura, H., Tanaka, Y., Ogasawara, T., Okada, K., Shiba, N., Sakamoto, K., et al. (2016). Allogeneic transplantation of iPS cell-derived cardiomyocytes regenerates primate hearts. Nature *538*, 388–391.

Shore, E.M., Xu, M., Feldman, G.J., Fenstermacher, D.A., Cho, T.J., Choi, I.H., Connor, J.M., Delai, P., Glaser, D.L., LeMerrer, M., et al. (2006). A recurrent mutation in the BMP type I receptor ACVR1 causes inherited and sporadic fibrodysplasia ossificans progressiva. Nat. Genet. *38*, 525–527.

Smith, Z.D., Sindhu, C., and Meissner, A. (2016). Molecular features of cellular reprogramming and development. Nature reviews. Mol. Cell. Biol. *17*, 139–154.

Soufi, A., Donahue, G., and Zaret, K.S. (2012). Facilitators and impediments of the pluripotency reprogramming factors' initial engagement with the genome. Cell *151*, 994–1004.

Soufi, A., Garcia, M.F., Jaroszewicz, A., Osman, N., Pellegrini, M., and Zaret, K.S. (2015). Pioneer transcription factors target partial DNA motifs on nucleosomes to initiate reprogramming. Cell *161*, 555–568.

Takahashi, K., Tanabe, K., Ohnuki, M., Narita, M., Ichisaka, T., Tomoda, K., and Yamanaka, S. (2007). Induction of pluripotent stem cells from adult human fibroblasts by defined factors. Cell *131*, 861–872.

Takahashi, K., Tanabe, K., Ohnuki, M., Narita, M., Sasaki, A., Yamamoto, M., Nakamura, M., Sutou, K., Osafune, K., and Yamanaka, S. (2014). Induction of pluripotency in human somatic cells via a transient state resembling primitive streak-like mesendoderm. Nat.Commun. *5*, 3678.

Takahashi, K., and Yamanaka, S. (2006). Induction of pluripotent stem cells from mouse embryonic and adult fibroblast cultures by defined factors. Cell *126*, 663–676.

Takahashi, K., and Yamanaka, S. (2016). A decade of transcription factor-mediated reprogramming to pluripotency. Nature reviews. Mol. Cell Biol. *17*, 183–193.

Tan, L., Ke, Z., Tombline, G., Macoretta, N., Hayes, K., Tian, X., Lv, R., Ablaeva, J., Gilbert, M., Bhanu, N.V., et al. (2017). Naked mole rat cells have a stable epigenome that resists iPSC reprogramming. Stem Cell Rep. *9*, 1721–1734.

Vassena, R., Boue, S., Gonzalez-Roca, E., Aran, B., Auer, H., Veiga, A., and Izpisua Belmonte, J.C. (2011). Waves of early transcriptional activation and pluripotency program initiation during human preimplantation development. Development *138*, 3699–3709.

Vinogradova, M., Gehling, V.S., Gustafson, A., Arora, S., Tindell, C.A., Wilson, C., Williamson, K.E., Guler, G.D., Gangurde, P., Manieri, W., et al. (2016). An inhibitor of KDM5 demethylases reduces survival of drug-tolerant cancer cells. Nat. Chem. Biol. *12*, 531–538.

Wang, J., Xie, G., Singh, M., Ghanbarian, A.T., Rasko, T., Szvetnik, A., Cai, H., Besser, D., Prigione, A., Fuchs, N.V., et al. (2014). Primate-specific endogenous retrovirus-driven transcription defines naive-like stem cells. Nature *516*, 405–409.

Wang, L., Chang, J., Varghese, D., Dellinger, M., Kumar, S., Best, A.M., Ruiz, J., Bruick, R., Pena-Llopis, S., Xu, J., et al. (2013). A small molecule modulates Jumonji histone demethylase activity and selectively inhibits cancer growth. Nat.Commun. *4*, 2035.

Watanabe, K., Ueno, M., Kamiya, D., Nishiyama, A., Matsumura, M., Wataya, T., Takahashi, J.B., Nishikawa, S., Nishikawa, S., Muguruma, K., et al. (2007). A ROCK inhibitor permits survival of dissociated human embryonic stem cells. Nat.Biotechnol. *25*, 681–686.

Weitzel, K.W., Wickman, J.M., Augustin, S.G., and Strom, J.G. (2000). Zaleplon: a pyrazolopyrimidine sedative-hypnotic agent for the treatment of insomnia. Clin.Ther. *22*, 1254–1267.

Xie, L., Pelz, C., Wang, W., Bashar, A., Varlamova, O., Shadle, S., and Impey, S. (2011). KDM5B regulates embryonic stem cell self-renewal and represses cryptic intragenic transcription. EMBO J. *30*, 1473–1484.

Xie, M., Tang, S., Li, K., and Ding, S. (2017). Pharmacological reprogramming of somatic cells for regenerative medicine. Acc. Chem. Res. *50*, 1202–1211.

Yamanaka, S. (2009). Elite and stochastic models for induced pluripotent stem cell generation. Nature *460*, 49–52.

Yamanaka, S., and Blau, H.M. (2010). Nuclear reprogramming to a pluripotent state by three approaches. Nature *465*, 704–712.

Yu, J.Y., Vodyanik, M.A., Smuga-Otto, K., Antosiewicz-Bourget, J., Frane, J.L., Tian, S., Nie, J., Jonsdottir, G.A., Ruotti, V., Stewart, R., et al. (2007). Induced pluripotent stem cell lines derived from human somatic cells. Science *318*, 1917–1920.

ISCI, Volume *12*

Supplemental Information

Imidazopyridines as Potent KDM5 Demethylase Inhibitors Promoting Reprogramming Efficiency of Human iPSCs

Yasamin Dabiri, Rodrigo A. Gama-Brambila, Katerina Taškova, Kristina Herold, Stefanie Reuter, James Adjaye, Jochen Utikal, Ralf Mrowka, Jichang Wang, Miguel A. Andrade-Navarro, and Xinlai Cheng

Results

Table S1. Chemical structures of O4I3 derivatives, related to Figure 1.

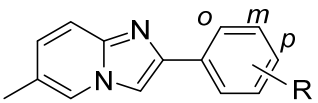

NO.	R
1 (O4I3)	*p*-CH_3
2	*p*-F
3	*p*-Cl
4	*p*-Br
5	*p*-NO_2
6	*p*-OMe
7	*p*-OH
8	*p*-CN
9	*m*-NO_2
10	*o*-NO_2
11	*m*-F
12	*o*-F

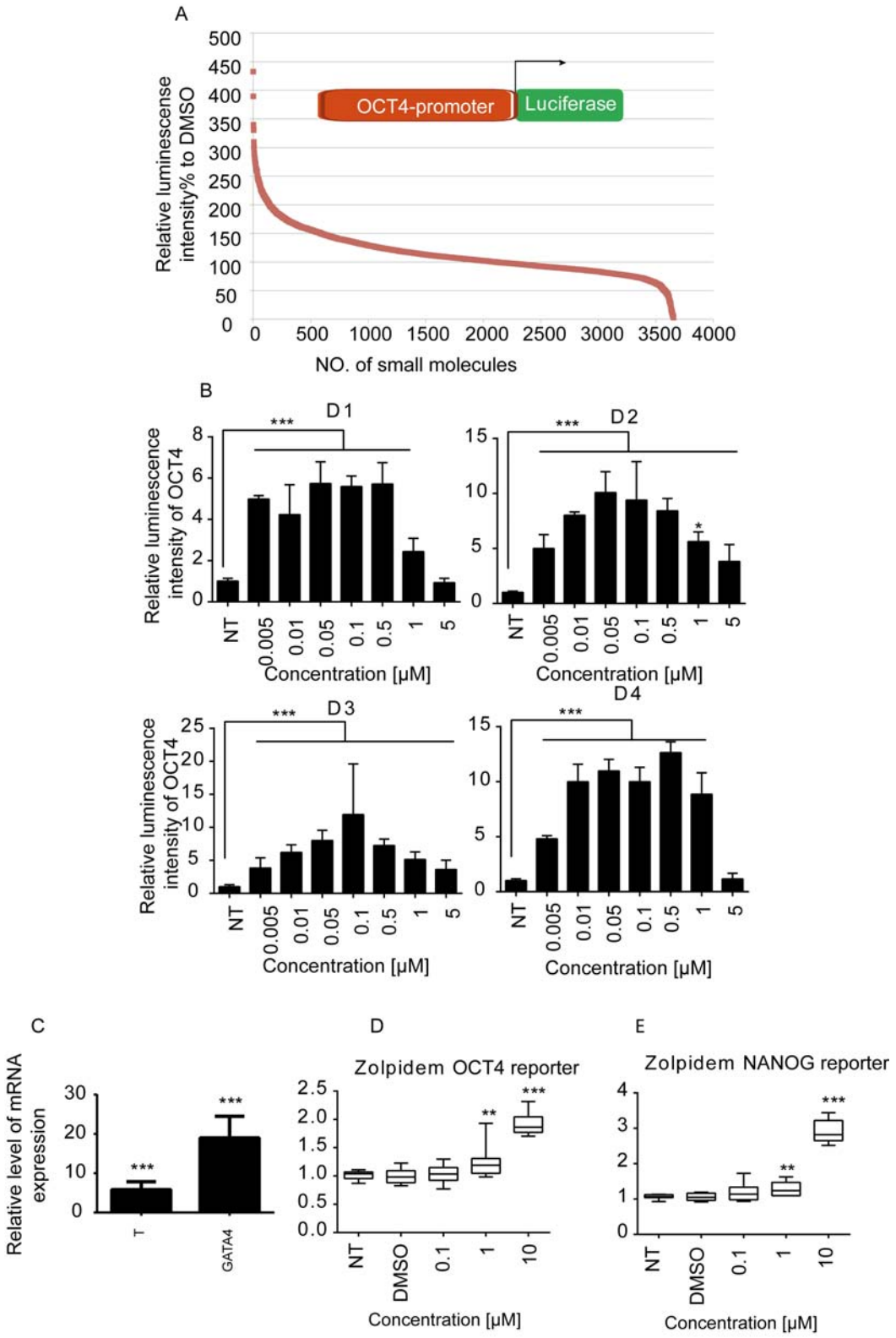

Figure S1. Identification of imidazopyridine analogues as OCT4 inducing compounds, related to Figure 1. (A) Imidazopyridines influence OCT4 expression in HEK293-OCT4 promoter-driven luciferase reporter cells using cell-based high throughput screening. **(B)** O4I3 activates OCT4 in NCCIT-OCT4 reporter cells at day 1, 2, 3, and 4. **(C)** High dose of O4I3 (10 μM) induces PSCs differentiation detected by expression of T and GATA4.

(D) Zolpidem (10 μM, 48 h) activates OCT4 in NCCIT-OCT4 and **(E)** NANOG in NCCIT-NANOG reporter cells. In **(B-E)** statistical significance was compared to mock (0.1% DMSO) treatment using tow-way ANOVA and a post-hoc Tukey test. Data are represented as mean ± SD. ***: $p<0.001$, **: $p<0.01$, and *: $p<0.05$.

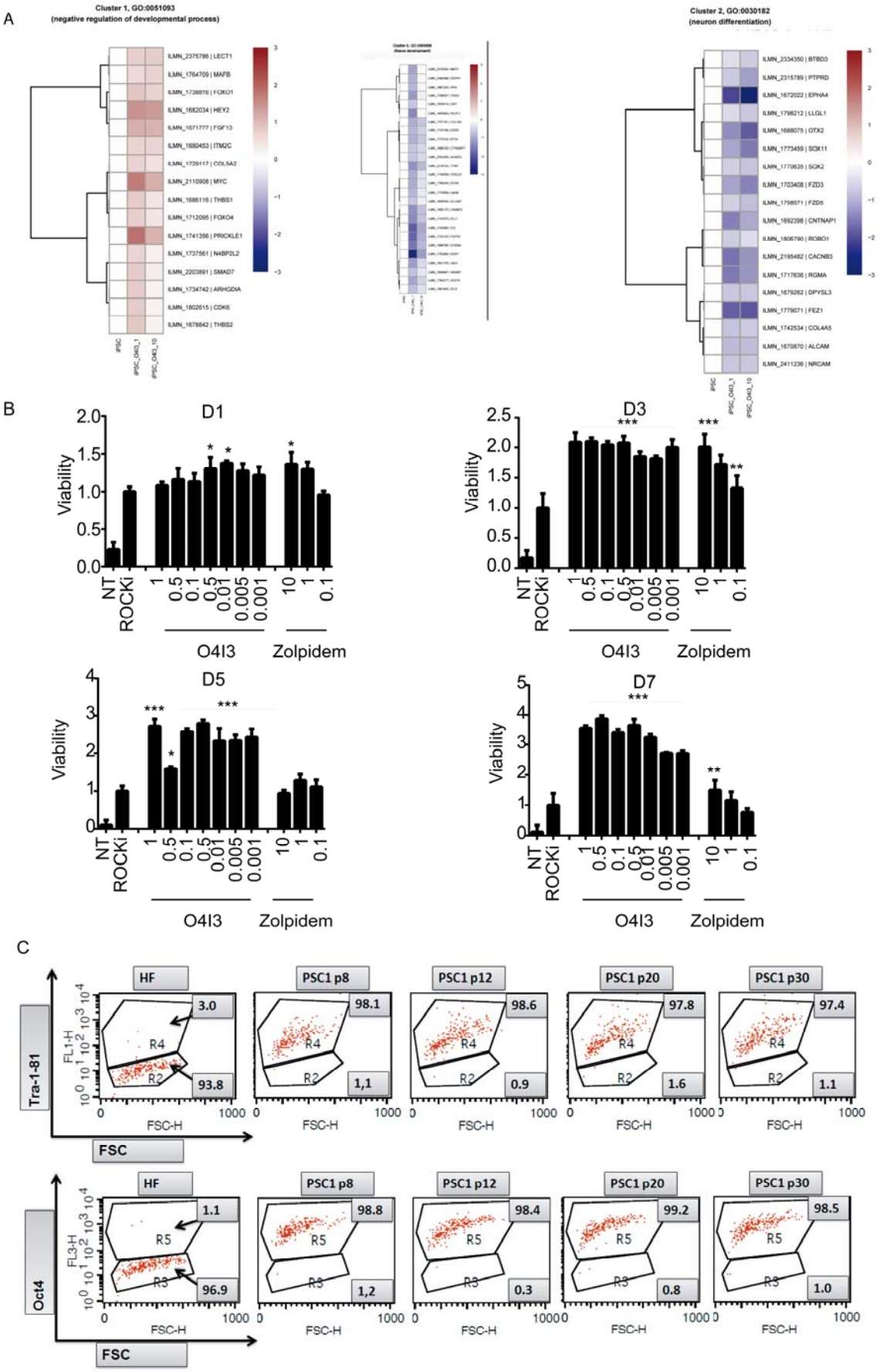
A
Cluster 1, GO:0051093
(negative regulation of developmental process)
Cluster 2, GO:0030182
(neuron differentiation)
B
D1
D3
D5
D7
Viability
NT
ROCKi
O4I3
Zolpidem
C
HF
PSC1 p8
PSC1 p12
PSC1 p20
PSC1 p30
Tra-1-81
Oct4
FL1-H
FL3-H
FSC-H
FSC
R4
R2
R5
R3
3.0
93.8
98.1
1,1
98.6
0.9
97.8
1.6
97.4
1.1
1.1
96.9
98.8
1,2
98.4
0.3
99.2
0.8
98.5
1.0

Figure S2. O4I3 supports maintenance of hPSCs, related to Figure 1. (A) Gene expression profiles of gene sets enriched in selected Gene Ontology categories related to pluripotency, development, and homeostasis in O4I3-treated iPSCs for 24 h at 1 nM (iPSC_O4I3_1) and 10 nM (iPSC_O4I3_10). The genes belong to two out of three statistically significant gene clusters found with STEM. **(B)** O4I3 increases the viability of hPSCs after single cell expansion using ROCK inhibitor (ROCKi; 10 μM) for the first 24 h followed by continuous cultivation for 7 days in the presence of various concentrations of O4I3, determined by MTT assay. **(C)** Stable expression of pluripotency markers, TRA-1-81 and OCT4 in hPSCs in the presence of O4I3 (10 nM) till at least passage NO. 30, detected by FACS analysis. Data in **(B)** represent mean ± SD from at least 3 independent experiments. Data in **(B)** represent mean ± SD from at least 3 independent experiments. In **(B)** significance was compared to mock (0.1% DMSO) treatment using two-way ANOVA and a post-hoc Tukey test. Data represent mean ± SD from at least 3 independent experiments.***: $p<0.001$, **: $p<0.01$, and *: $p<0.05$.

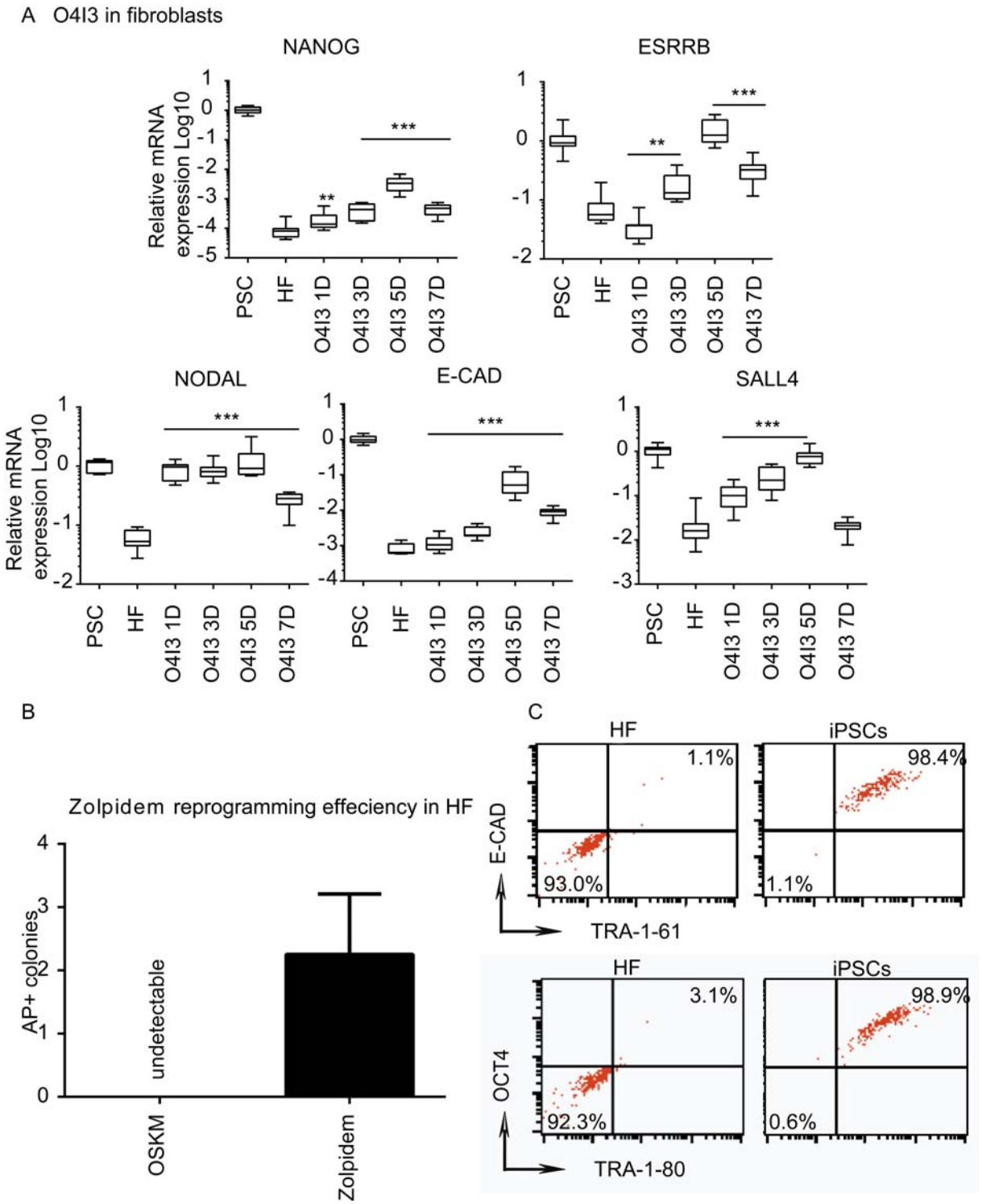

Figure S3. O4I3 and zolpidem enhance the efficiency of OSKM-induced reprogramming, related to Figure 2. (A) O4I3 induces reprogramming-associated gene expression, NANOG, ESRRB, NODAL, CDH1, and SALL4, detected by qPCR. **(B)** AP+ colonies were found in resistant fibroblasts (HF4) treated with zolpidem in combination with episomal expression of OSKM. **(C)** Expression of pluripotency markers, E-Cadherin (E-CAD), TRA-1-61, OCT4 and TRA-1-80 in HF, and the newly generated iPSCs. In **(A)** statistical significance was compared to mock (0.1% DMSO) treatment using two-way ANOVA followed by a post-hoc Tukey test. Data in **(A)** and **(B)** bar plots are represented as mean ± SD from at least 3 independent experiments. ***: $p<0.001$, **: $p<0.01$, and *: $p<0.05$.

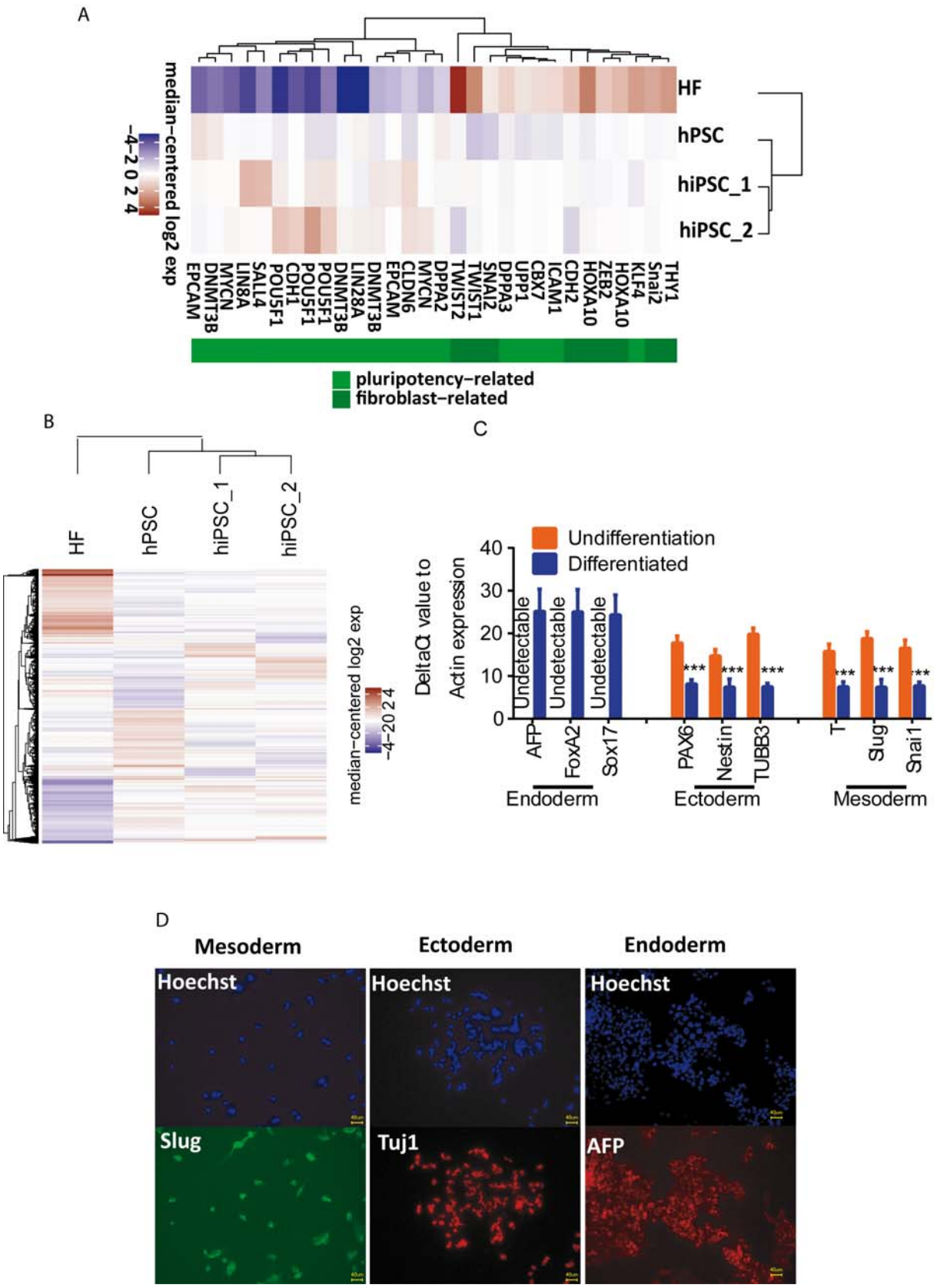

Figure S4. Newly generated iPSCs with ectopic expression of OSKM in combination with O4I3 are pluripotent, related to Figure 2. (A) Heatmap of gene expression profiles of selected pluripotency-associated genes (labled with bright green) and fibroblast-associated genes (labled with dark green) expression. The cells in both heatmaps depict log2 transformed gene expression values, centred on the gene-specific median expression

across all samples. Genes and samples are reordered using hierarchical clustering based on complete linkage and Euclidean distance. Heat map shows similar expression patterns of pluripotency- and fibroblast-related genes between hPSC (positive control) and the newly generated iPSCs (hiPSC_1 and hiPSC_2), which are distinct from those of fibroblast (HF). **(B)** Heatmap of global gene expression profiles. HF: human fibroblasts; hPSC: positive control, hiPSC_1: newly generated human iPSCs 1. hiPSC_2: newly generated human iPSCs 2. **(C)** Expression of differentiation markers for three germ layers, analyzed by qPCR and **(D)** immunocytochemistry using standard differentiation protocols. Scale bar: 40 μm. In **(C)** statistical significance was compared to undifferentiated iPSCs using two-way ANOVA and a post-hoc Tukey test. Data in **(C)** are represented as mean ± SD from at least 3 independent experiments. ***: $p<0.001$.

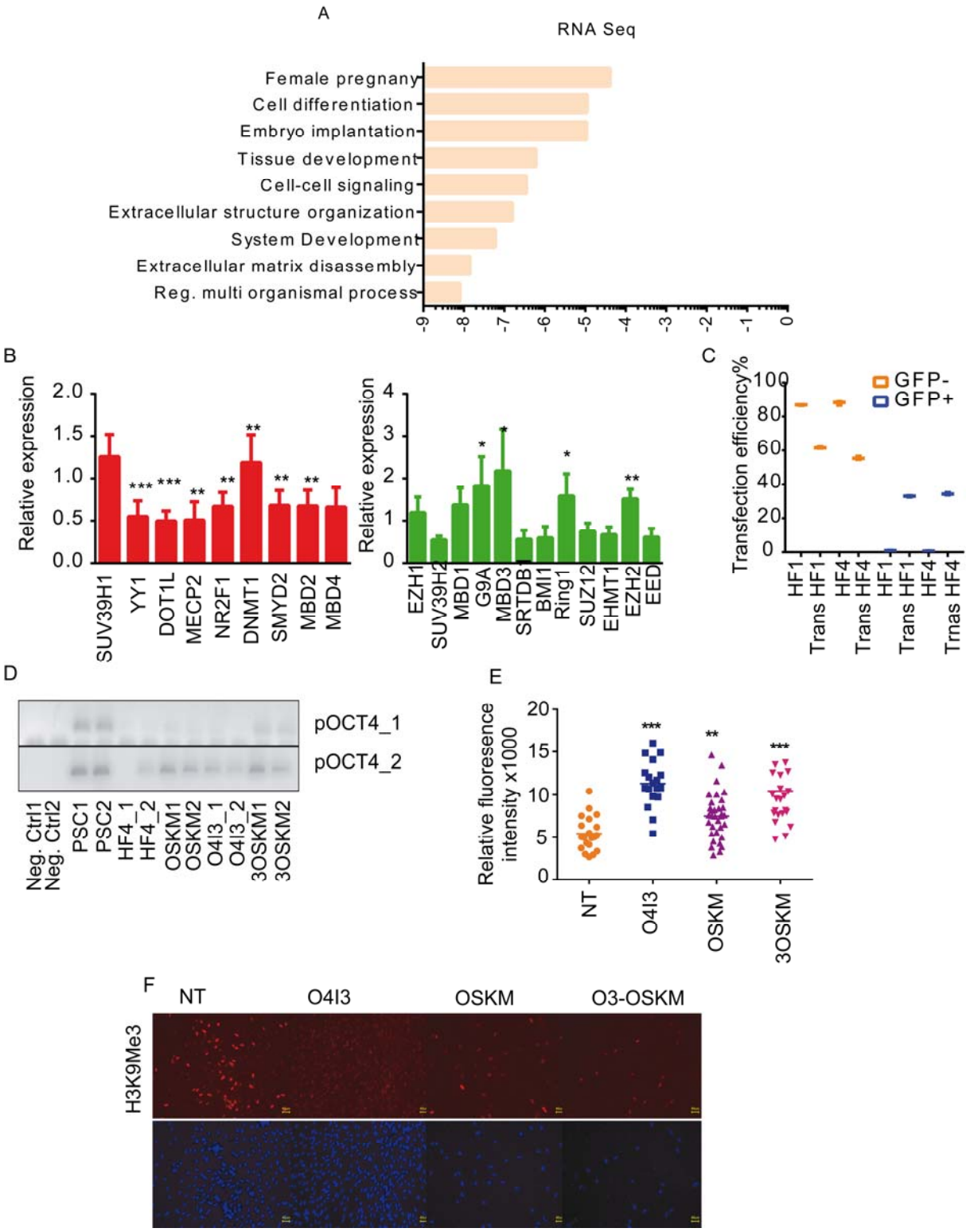

Figure S5. O4I3 is an epigenetic modulator, related to Figure 3. (A) Functional enrichment analysis of differentially expressed genes in O4I3-treated HF and mock treatment obtained from RNA-Seq experiment. **(B)** O4I3-regulated genes involved in histone modification and chromatin remodelling, as described by Onder et al.(Onder et al., 2012) using qRT-PCR in fibroblasts treated with O4I3 at a concentration of 250 nM for 48 h. Red indicates potential reprogramming inhibitors, whereas green color represents the potential activators. **(C)** Comparison of transfection efficiency in HF1 and HF4 using an episomal EGFP vector (Trans HF; transfected fibroblasts). **(D)** Enrichment of H3K4Me3 at the promoter of OCT4 analyzed by Chip-qPCR, the PCR-products

were detected in 1.5% agarose gel. **(E)** Abundance of H3K4Me3 in HF cells treated with O4I3 (250 nM for 24 h), transfected with OSKM or incubated with the combination of both, detected by immunocytochemistry using H3K4Me3 antibody. **(F)** Reduction of H3K9Me3 upon O4I3 treatment for 48 h. The significance was compared to mock (0.1% DMSO) treatment using two-way ANOVA and a post-hoc Tukey test. Data in **(A)**, **(B)**, **(C)**, and **(E)** represent mean ± SD from at least 3 independent experiments. ***: p<0.001, **: p<0.01, and *: p<0.05.

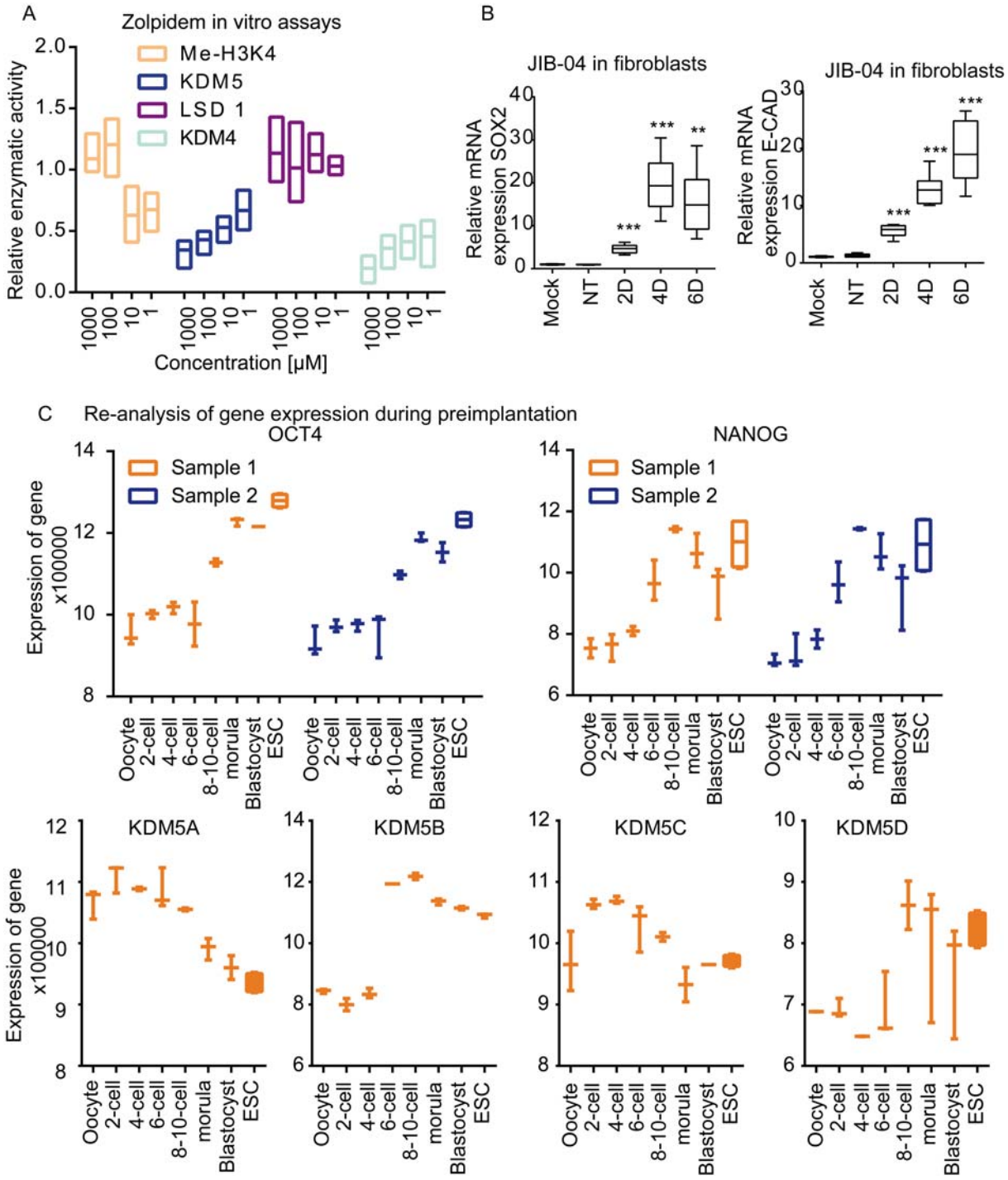

Figure S6. KDM5 demethylases play an important role in the induction of pluripotency, related to Figure 4. (A) Zolpidem inhibits KDM5 activity and protects methylation of H3K4 in vitro. The inhibitory effect of zolpidem on KDM5, methylated H3K4, LSD1 and KDM4 was measured. **(B)** JIB-04 (5 μM, 48 h) induces

SOX2 and CDH1, encoding E-Cadherin (E-CAD), mRNA levels in fibroblasts. **(C)** Comparison of KDM5s' expression patterns with those of pluripotency markers, OCT4 and NANOG at different stages during the human preimplantation development as described previously (Vassena et al., 2011). The statistical significance was compared to mock (0.1% DMSO) treatment using two-way ANOVA and a post-hoc Tukey test. Data represent mean ± SD from at least 3 independent experiments. ***: $p<0.001$ and **: $p<0.01$.

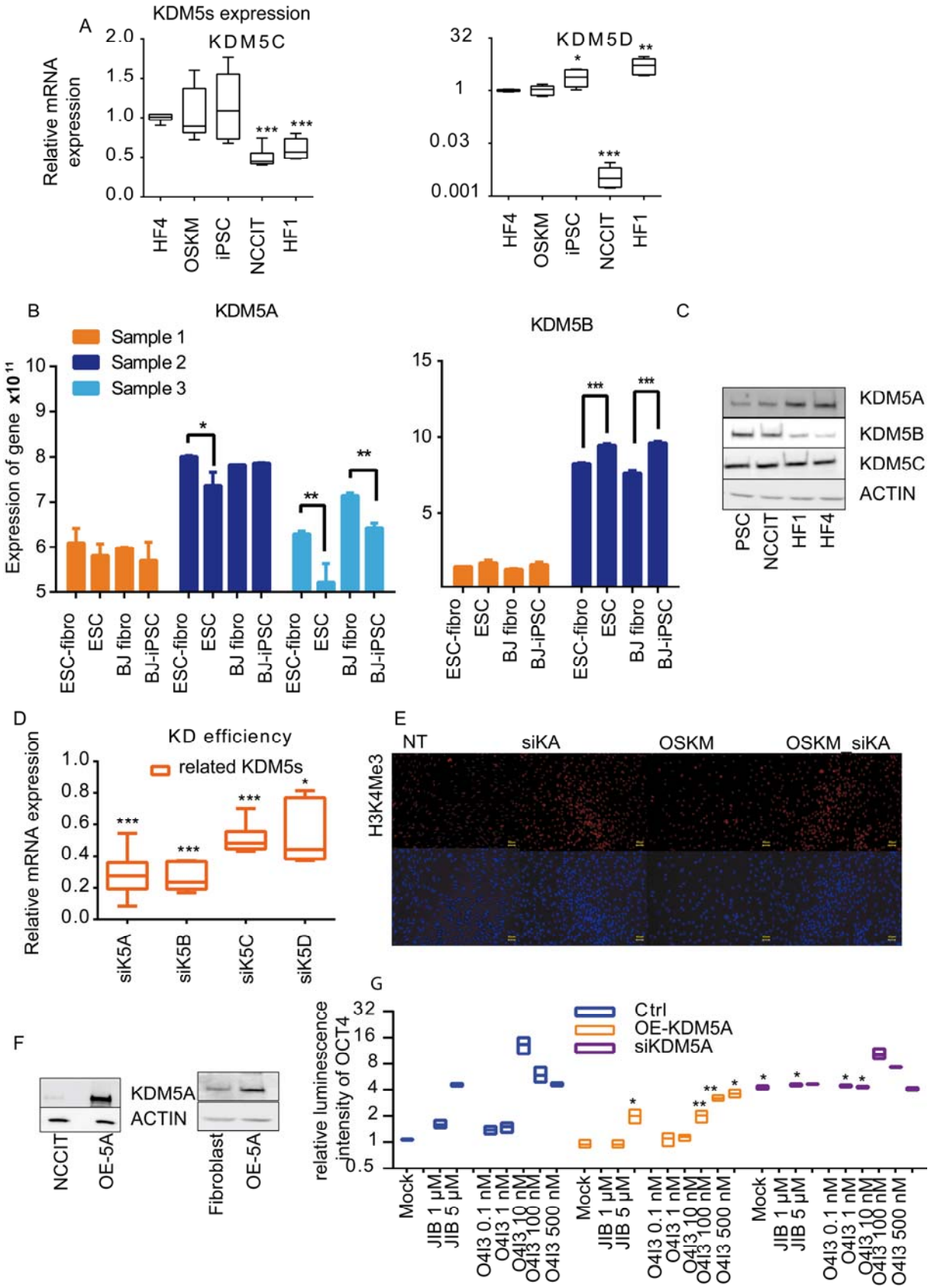

Figure S7. KDM5 demethylases play an important role in the induction of pluripotency, related to Figure 4. (A) Comparison of KDM5C and KDM5D expression in reprogramming-resistant fibroblasts (HF4), transfected with OSKM, iPSCs, NCCIT and HF1, determined by qRTPCR. **(B)** Comparison of KDM5A and KDM5B expression levels in pluripotent stem cells and related fibroblasts. Previously reported data were

used(Takahashi et al., 2014). **(C)** Expression of KDM5A, KDM5B, and KDM5C at the protein level in PSC, NCCIT, HF4 and HF1. KDM5D was undetectable in all four cell lines. **(D)** Knock-down (KD) efficiencies of siRNA (si)-mediated repression of KDM5s in fibroblasts, as determined by qRT-PCR. **(E)** Global elevation of H3K4Me3 expression caused by knock-down of KDM5A (20 nM of anti-KDM5A siRNA: siKA). **(F)** Overexpression efficiency of KDM5A (Overexpressed KDM5A: OE-5A) in NCCIT and fibroblast cells. **(G)** Overexpression (OE-KDM5A) or knockdown (siKDM5A) of KDM5A influenced the activity of KDM5A inhibitors (JIB-04 and/or O4I3) in NCCIT-OCT4 reporter cells after 48 h of treatment at the indicated concentrations. The statistical significance was compared to either mock (0.1% DMSO) or non-targeting siRNA treatment using two-way ANOVA and a post-hoc Tukey test. Data are represented as mean ± SD from at least 3 independent experiments. ***: $p<0.001$, **: $p<0.01$, and *: $p<0.05$.

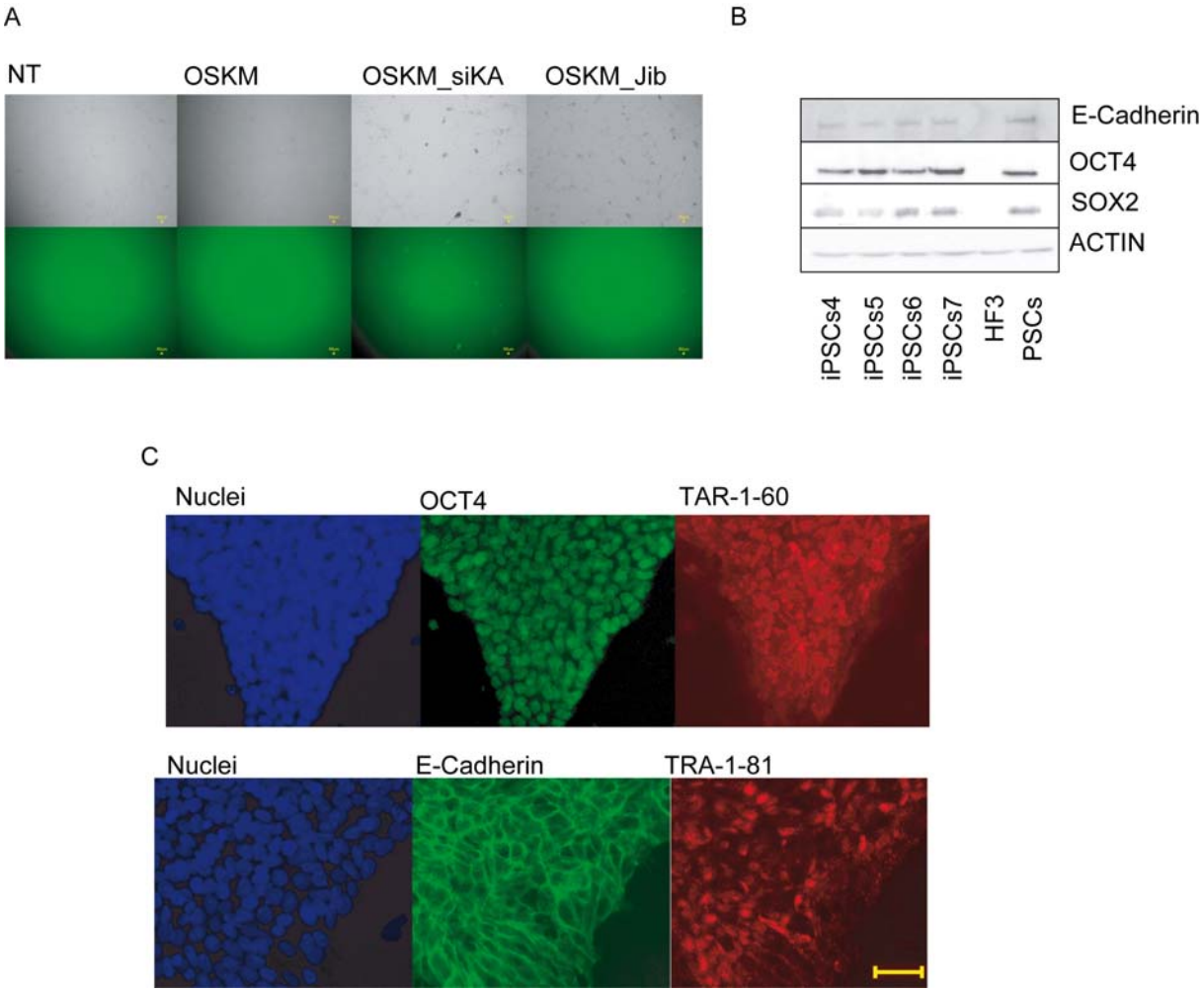

Figure S8. KDM5A is a pluripotency inhibitor, related to Figure 5. (A) LTR-7-GFP positive ESC-like colonies were found in resistant fibroblasts in the presence of either anti-KDM5A siRNA (siKA) or JIB-04 in combination with OSKM but not in cells transfected with OSKM alone. **(B)** Comparison of E-Cadherin, OCT4 and SOX2 protein expression in reprogramming-resistant fibroblasts (HF3), iPSC_4-7 which were generated by means of episomal expression of OSKM and repression of KDM5A activity, and PSCs (as positive control). **(C)** Co-expression of OCT4 and TRA-1-60 as well as E-Cadherin and TRA-1-81 in iPSCs. Scale bar: 40 μm.

TRANSARENT METHODS

Chemicals and reagents

The compound O4I3 was not identified as a pan assay interference compounds (PAINS), as previously described (Cheng et al., 2017). Histone demethylase inhibitors were purchased from Cayman Chemical (Biomol, Germany). Small interfering RNA against KDM5A (oligo ID: 107607), KDM5B (oligo ID: 108065), KDM5C (oligo ID: 14315), and KDM5D (oligo ID: 107493) were purchased from Thermofisher Scientific (Germany). Lipofectamin 3000 (Life Technologies, Thermofisher Scientific) was used for transfection.

Luciferase reporter Assay

Luciferase reporter assay was performed using beatle juice kit (PJK, Germany) according to the manufacturer's instruction as previously described (Cheng et al., 2015a; Cheng et al., 2015b). NCCIT-OCT and NCCIT-Nanog reporter cells were plated into a 24-well plate (100,000 cells/well) for 24 h. Cells were treated with compounds as indicated and harvested with luciferase lysis buffer (25 mM Tris phosphate buffer pH=7.8 containing 4 mM EGTA, 1% Triton X-100, 10% glycerol, and 2mM fresh DTT, filtered through 0.45 µm sterile filter) at 37°C for 15 min. The protein concentration was determined by Bradford reagent (Sigma-Aldrich, Germany). 100 µL reaction mixture containing luciferin and ATP was added to 20 µL cell lysis in a white plate (Gibco, Germany), incubated for 5 min and measured by Tecan Ultra plate reader (Tecan, Germany). The activity was determined as percentage luminescence intensity of treated- over control cells from at least five-independent experiments.

Quantitative Real Time (qRT) PCR

qRT-PCR was performed using a Light Cycler 96 (Roche, Germany) following the manufacturer's protocol. Briefly, total RNA was isolated from cells using QIAzol reagent

(Qiagen, Germany) or NulceoSpin®RNA Plus (Macherey-Nagel, Germany). The same amount of RNA was used to reverse-transcriptionally synthesize cDNA by using ProtoScript® First Strand cDNA Synthesis Kit (NEB, Germany). qPCR was performed using the SYBR Green PCR master mix (qPCRBIO SyGreen Mix Lo-Rox, Nippon Genetics, Germany) and the respective primer pairs (Eurofin Genomics, Germany) listed in Table List of the sequences of primer pairs. Actin was used as an endogenous control. Data were normalized to the value of untreated cells, showing the mean ± SD of quadruplicates and are representative of at least three independent experiments.

Immunoblotting

iPSCs were lysed using a urea-based lysis buffer (containing 1 mM EDTA, 0.5% Triton X-100, 5 mM NaF, 6 M Urea, and supplemented with protease inhibitors; 1 mM Na_3VO_4, 10 µg/mL pepstatin, 100 µM PMSF and 3 µg/mL aprotinin). Protein concentration was determined using Bradford reagent (Sigma-Aldrich). 40 µg of total protein was resolved on a 12% SDS-PAGE gel, thereafter transferred onto a PVDF membrane (GE Healthcare, Germany), then blocked with 5% milk in TBST (Tris-Buffered Saline Tween-20) for at least 1 h at room temperature followed by incubation with the respective primary antibodies (at a concentration of 1:1000 prepared in 5% milk/BSA TBST) at 4°C overnight. To visualize target proteins, membranes were further incubated with the horseradish peroxidase (HRP)-linked secondary antibodies (Cell Signaling Technologies) prepared in 5% milk TBST for 1 h at room temperature. Signals were detected by Western Lightning Plus ECl (Perkin Elmer, Germany) using the Fujifilm LAS-3000 imaging system. ß-Actin antibody was used as loading control. Primary antibodies used in this study are listed in Table list of primary antibodies.

Immunocytochemistry

iPSCs were seeded in 96-well plates coated with Geltrex (Life Technologies) at a density of 10,000 cells/well. Cells were fixed with 4% paraformaldehyde (PFA) at room temperature for 15 min, and blocked with blocking buffer (5% goat serum and 0.3% Triton X-100 in PBS) for 1 hr. Blocking solution was aspirated and replaced with the respective antibodies prepared in antibody dilution buffer (1% BSA and 0.2% Triton X-100 in PBS), then incubated at 4°C overnight. On the following day, cells were further incubated with the secondary antibodies (Goat anti-rabbit Alexa Flor 488 and Goat anti-mouse Alexa Flor 594, Dianova, Germany) for 1h, and were imaged using BIOREVO fluorescence microscope (BZ9000, KEYENCE, Germany). Hoechst 33342 (1 µg/mL in PBS, Sigma-Aldrich) was used to visualize nuclei.

FACS analysis of pluripotency markers

iPSCs were seeded in 6-well plates coated with Geltrex at a density of 300,000 cells/well. Cells were harvested on the following day, fixed and permeabilized by incubation with 4% PFA at room temperature for 15 min. Fixed cells were then incubated with the respective primary antibody at 4°C and further with the secondary antibody (Goat anti-rabbit Alexa Flor 488 and Goat anti-mouse Alexa Flor 594) for 1 h at room temperature, and immediately measured by FACSCalibur (Becton Dickinson, USA). Data were analyzed by the software, CellQuest Pro (Becton Dickinson).

TRA-1-60+ colonies counting

To assess the number of TRA-1-60+ colonies, 10,000 fibroblast cells/well in 96-well plates were transfected with episomal OSKM (Epi5 kit, Thermofisher Scientific) in the presence/absence of small molecules, as indicated in the text. Immunostaining was performed using TRA-1-60 antibody in living cells after 32 days. Transfection efficiency was indicated by quantifying the expression of EGFP (Addgene plasmid # 27082).

iPSCs differentiation

Cellartis iPS cell to hepatocyte differentiation system (Takara, Germany) was used for differentiation of iPSCs to endoderm. StemDiff neuron differentiation kit (08500, Stem Cell Technologies, Germany) was used for differentiation of iPSCs to neuroectoderm. To differentiate iPSCs to mesoderm, cells were seeded in Geltrex-coated plates as single cells and cultivated till the density reached to at least 80%. N2+B27 medium was used to replace E8 medium. Activin (100 ng/mL), bFGF (20 ng/mL), BMP4 (10 ng/mL), Ly2 (10 μM) and Chir (5 μM) were freshly added. The medium was changed every two days for 14 days.

Measurement of methylated H3K4 and the in vitro activity of LSD1, KDM4, and KDM5 demethylases

Epiquik histone demethylase (H3K4 specific) activity/inhibition assay kit (Epigentek, Biocat, Germany) was used to measure the protective effect of O4I3 and zolpidem on the methylation of H3K4. Their inhibitory effects on LSD1, KDM5s, and KDM4 were determined using Epigenase jarid demethylase activity/inhibition assay kit, Epigenase JMJD2 demethylase activity/inhibition assay kit and EpiQuik histone demethylase LSD1 activity/inhibition assay kit (Epigentek, Biocat, Germany). The total nuclear extraction was used according to manufacturer's instructions. For measuring KDM5A, KDM5B, KDM5C, and KDM5D activity, magnetic beads were used to immunoprecipitate the respective enzymes from 10^8 cells according to the manufacturer's instructions (Cell Signaling Technologies).

Chromatin immunoprecipitation assay

SimpleChIP Plus Enzymatic Chromatin IP Kit (Cell Signaling Technologies) was used to isolate DNA precipitated with H3K4Me3 or H3K27Me3 antibody. According to the manufacturer's protocol, 10^6 cells/sample were collected. Non-target Rabbit IgG and total Histone H3 antibodies (provided in the kit) were used as negative and positive controls,

respectively. KDM5A-D enzymes were purified using immunoprecipitation with magnetic beads according to the manufacture's protocol. Recruited DNA was subjected to qRT-PCR using ChIP primers sets, and human RPL30 exon 3 primer pairs were used as positive control.

Gene expression profiling and data analysis

Gene expression profiling of human PSCs, iPSCs and fibroblast samples was conducted on the Illumina Human Sentrix-12v4 BeadChip array by the Genomics and Proteomics Core Facility of DKFZ. Two sets of samples were profiled: (i) three hPSC samples, corresponding to treatments with two O4I3 doses (1 nM and 10 nM) and not-treated hPSCs; (ii) three fibroblast samples, corresponding to two treatments (one with O4I3 and one with OSKM) and not-treated fibroblast.

Gene expression analysis was performed in R 3.3.2 computing environment and mainly packages from the open-source software development project Bioconductor 3.4 (Gentleman et al., 2004) In addition, we used the standalone tool STEM 1.3.11 for clustering of gene profiles (and functional enrichment analysis), and STRING 10.5 for building protein-protein interaction networks (Szklarczyk et al., 2016). Quality assessment and preprocessing of raw data was done with the package beadarray 2.24.2 (Dunning et al., 2007). Prepossessing involved default image processing (with median-based local background), default Illumina removal for outlying observations, mean summarization of bead-level observations into probe-level data, quantile normalization of probe-level data and log2 transformation. The resulting probes were matched to genes using annotations from the package illuminaHumanv4.db 1.26.0. We filtered probes that poorly matched the annotated genes (quality status of 'no-match' and 'bad') as well as low-expression probes (detection score > 0.05, across all samples).

Dose experiment data analysis; 14108 probes were available for clustering analysis with STEM, a tool for clustering short time series data that can differentiate between real and random temporal expression patterns. For this purpose, we selected one probe per gene (the one with highest variance, if multiple probes matched to single gene) and converted the data into fold changes with respect to the not-treated iPSCs. We analyzed the data as short time series of length three (corresponding to dose level of 0, 1, and 10 nM), by treating dose level as time factor. We applied STEM in default mode, except for the following settings; at least one measurement with absolute fold change of 0.65; significance of model profiles corrected by False Discovery Rate method; cellular component terms, terms with evidence code IEA and NAS or terms that had less than 10 genes in-common with the identified model profiles (or clusters of similar model profiles) were excluded from the Gene Ontology (GO) enrichment analysis (Ashburner et al., 2000); multiple testing correction of GO term significance values were determined by the randomization test, with 5000 randomly sampled gene sets per term. Expression profiles of selected gene sets (related to significantly enriched GO terms) were visualized by heatmaps with the packages heatmap 1.0.8.

Fibroblast/iPSC experiment data analysis; approximately 18 000 probes, after filtering, were available for differentially expression analysis. The latter was based on fold changes, i.e., the probes with at least two-fold expression relative to the untreated fibroblast were selected as differentially expressed; since single biological replicates per treatment were used, statistical tests were not applicable. Global gene expression comparison between pairs of samples were visualized by scatter plots, plotted with the package ggplot2 2.2.1, while the heatmaps of gene expressions were visualized with the package ComplexHeatmap 1.12.0. In addition, columns and rows in the heatmaps were reordered with hierarchical clustering based on average linkage and Euclidean distance or Pearson correlation. Functional enrichment analysis on differentially expressed probes was performed with gProfileR version r1732_e89_eg36 via

the R interface in the package gProfileR version 0.6.1. More specifically, the query lists were treated as unordered human gene lists, and the set of probes retained after filtering was supplied as a background. Multiple testing correction was done by the FDR method according to Benjamini and Hochberg (Benjamini and Hochberg, 1995) with 0.05 FDR cut-off, including biological processes and molecular functions from the Gene Ontology database (Ashburner et al., 2000) with size of 5 up to 500 genes.

Statistics

Statistical and graphical analyses of the data (except microarray gene expression profiles) were performed using Prism software (two-way ANOVA test), considering p-values less than or equal to 0.05 as statistically significant.

List of the sequences of primer pairs.

Gene	F	R
Oct4	gaaggatgtggtccgagtgt	gtgaagtgagggctcccata
Sox2	aaccccaagatgcacaactc	gcttagcctcgtcgatgaac
Nanog	aatacctcagcctccagcagatg	tgcgtcacaccattgctattcttc
Lin28A	gtggatgtctttgtgcaccag	gacacggatggattccagac
Klf4	ggacctggactttattctctcc	gataggtgaagctgcaggtg
Esrrb	ccttccaatcagctgccttc	gatctgcctgcctctctcat
Nodal	gtcgacatcacttgccagac	tggtcggatgaaactcctcc
FGF2	aggagtgtgtgctaaccgtt	cagttcgtttcagtgccaca
E-Cadherin	gagagactgggttattcctc	gatgctgtagaaaaccttgcc
Rex1	tggacacgtctgtgctcttc	gtcttggcgtcttctcgaac
Sall4	atttgtgggaccctcgacat	ggtaaaagctcgcccacaaa
FGF5	agtggtatgtggccctgaat	ctgctccgactgcttgaatc

TBX3	catcgctgtgactgcatacc	tctcttcggccatttccagt
ZMF534	tggcaaggtcttcaggcata	tgaactttccgatgccttgc
FGF4	tgagtgcacgttcaaggaga	gacactcggttccccttctt
GATA4	tccaaaccagaaaacggaag	ctgtgcccgtagtgagatga
GATA6	ccacaacacaacctacagcc	acgcctatgtagagcccatc
PAX6	gacttcagctgaagcggaag	ggtagatctattttggctgc
Sox7	accccaactacaagtaccgg	tactcacccctgtcctcctt
T	acccagttcatagcggtgac	ggattgggagtacccaggtt
AFP	agacatcctcagcttgctgt	aatgcttggctctcctggat
FoxA2	ctactcctccgtgagcaaca	gacgacatgttcatggagcc
Sox17	cagaatccagacctgcacaa	gcggccggtacttgtagtt
Nestin	tccaggaacggaaaatcaag	gcctcctcatcccctacttc
TUBB3	cagatgttcgatgccaagaa	gggatccactccacgaagta
Slug	ctcctctttccggatactcctc	gtagtctttcctctgagccac
Snail1	cctctacttcagtctcttcc	ctttcgagcctggagaattccttg
SUV39H1	attcgcaagaacagcttcgt	acacgtcctccacgtagtcc
YY1	ggataactcggccatgagaa	cgcaaattgaagtccagtga
hDOT1L	ccaaaactcagggaggaaca	cttcctcagcaccagagtcc
DNMT3A	attacccaatggggacttgg	cagccattttccactgctct
MECP2	gagaccgtactccccatcaa	agtcctttcccgctcttctc
NR2F1	tacgtgaggagccagtaccc	cctaccaaacggacgaagaa
DNMT1	gagctaccacgcagacatca	cgaggaagtagaagcggttg
hSMYD2	gaccctggcagaagtcagag	ggtggtacactcctggcact
MBD2	acgtcagcttttctgggaga	gcactggcaacagcagataa
MBD4	aggcaaaatggcaatacctg	gtttttgcccgaagatcgta

hEZH1	ctctgcactccttccacaca	ttccagcaaaaggaagcagt
SUV39H2	gatttagagggcccaccttc	gggagtaccaggtgggattt
MBD1	tgagaccaaggctgacactg	acattctctgttcccggttg
G9A	caaaatcgggaacttggaga	ctcgttgtcagtgagggtga
MBD3	ggccacagggatgtctttta	ttgacctggttggaggagtc
SETDB1	acatcctcagcctctgcact	ttccagtaccggtcagatcc
BMI1	ccagggcttttcaaaaatga	ccgatccaatctgttctggt
Ring1	cgggaacaaggagtgtccta	tcctcccggctaggatagat
SUZ12	aaacgaaatcgtgaggatgg	ccatttcctgcatggctact
EHMT1	ctgctgggagaagagacacc	gcatcgctgttttcacaaga
EZH2	ttcatgcaacacccaacact	gagagcagcagcaaactcct
EED	gagagggaagtgtcgactgc	ggtgtatcagggcgttcagt
Actin	ctgactacctcatgaagatcctc	cattgccaatggtgatgacctg
Oct4 promoter1	GTTTGTGTGTATGCATGCCA	AAGCTGCTAAGTTCTGGGTT
Oct4 promoter2	GGATATAGCACGGAGGCCTT	CACCCTCTCAGCTCCTCAAA

List of the primary antibodies.

Abs	Company	Cat#	Abs	Company	Cat#
Oct4A (30A3)	Cell signaling	2840S	H3K4Me3	Cell signaling	9751P
Sox2	Cell signaling	4900	H3K9Me3	Cell signaling	13969
Lin28	epitomics	3334-1	Slug	Cell signaling	9585P
E-Cadherin	Cell Signaling	3195	AFP	Cell signaling	9303P
ß-Catenin (D10A8) XP	Cell signaling	8480P	Tuj1	Promega	G7121
ß-Actin (C4)	santa cruz	sc-47778	KDM5A	Cell signaling	3876
Nanog (1E6C4)	Cell signaling	4893S	KDM5B	Cell signaling	3273
Tra-1-60 (S)	Cell signaling	4746P	KDM5C	Cell signaling	5361
Tra-1-81	Cell signaling	4745P	KDM5D	Thermofisher	PA5-40120
H3K27Me3	Cell signaling	9733			

Chemistry

Reagents

Solvents and reagents were obtained from commercial suppliers were at least of reagent grade and were distilled or dried according to prevailing methods prior to use, if necessary. For monitoring the reactions, Alugram SIL G/UV254 sheets for TLC (Macherey & Nagel) were used. Flash column chromatography was accomplished using silica gel 60 (Macherey & Nagel, 0.040-0.063 mm). The purity of compounds was determined at least more than 96% by HPLC analysis.

General procedure for the syntheses

A mixture of 5-methylpyridin-2-amine and 2-bromo-1-phenylethan-1-ones (2:1) in EtOH was stirred at 60°C for 3 h. TLC was employed to control the reaction. After removal of solvent the solid was suspended in 1N HCl and stirred for 2-3 h, filtered and washed with water to obtain the products in good yield (>90%).

Analytical Methods

^{1}H and ^{13}C NMR spectra were recorded on a Varian 300 MHz NMR system (^{1}H: 300 MHz, ^{13}C: 75 MHz). Chemical shifts are reported in ppm from tetramethylsilane with solvent as the internal standard (^{1}H DMSO-d_6: δ 2.50; ^{13}C DMSO-d_6: δ 39.5). The following abbreviations were used to explain the multiplicities in NMR spectra: s =singlet, d = doublet, t = triplet, q = quartet, m = multiplet. High-resolution mass spectra (HRMS) were recorded on a Bruker ApexQe hybrid 9.4 T FT-ICR (ESI).

6-Methyl-2-(p-tolyl)imidazo[1,2-a]pyridine (1, O4I3)

O4I3 1H NMR: δ 8.71 – 8.62 (m, 2H), 7.93 – 7.69 (m, 4H), 7.32 (d, J = 8.0 Hz, 2H), 2.41 – 2.24 (m, 6H). ^{13}C NMR: δ 140.60 , 139.13 , 136.12 , 135.63 , 130.29 , 127.49 , 126.82 , 126.48 , 123.94 , 111.57 , 110.67 , 21.39 , 17.85. HRMS (ESI) calculated m/z, 223,1230; found $C_{15}H_{15}N_2$ m/z, 223,1230 $[M + H]^+$. IR(cm^{-1}): 3342, 2159, 2021, 1661, 1540, 1534, 1527, 1505, 1456, 1366, 1360, 1311, 1269, 1195, 949, 848, 839, 805, 783, 767, 761, 740, 722.

2-(4-Fluorophenyl)-6-methylimidazo[1,2-a]pyridine (2)

^{1}H NMR: δ 8.83 – 8.54 (m, 2H), 8.30 – 7.88 (m, 2H), 7.90 – 7.65 (m, 2H), 7.55 – 7.17 (m, 2H), 2.38 (d, *J* = 1.1 Hz, 3H). ^{13}C NMR: δ 218.80 , 165.07 , 139.36 , 136.19 , 134.90 , 129.08 (d, *J* = 8.7 Hz), 127.48 , 126.87 , 117.05 , 116.75 , 111.73 , 111.08 , 17.84 . HRMS (ESI) calculated m/z, 227.0979; found $C_{14}H_{12}FN_2$; m/z, 227.0979 $[M + H]^+$. IR (cm^{-1}): 3325, 3114, 2524, 2362, 2165, 2017, 1659, 1501, 1446, 1271, 1238, 1165, 849, 823, 805, 788, 742.

2-(4-Chlorophenyl)-6-methylimidazo[1,2-a] pyridine (3)

^{1}H NMR: δ 8.76 (d, *J* = 0.6 Hz, 1H), 8.68 (q, *J* = 1.2 Hz, 1H), 8.07 – 7.99 (m, 2H), 7.89 – 7.73 (m, 2H), 7.65 – 7.56 (m, 2H), 2.39 (d, *J* = 1.1 Hz, 3H). ^{13}C NMR: δ 139.50 , 136.29 , 135.23 , 134.75 , 129.83 , 128.34 , 127.50 , 126.88 , 126.02 , 111.83 , 111.60 , 109.98 , 17.86. HRMS (ESI) calculated m/z, 243.0684; found $C_{14}H_{12}ClN_2$ m/z, 243.0684 $[M + H]^+$. IR (cm^{-1}): 3303, 2528, 2362, 2162, 2020, 1660, 1527, 1488, 1474, 1455, 1416, 1273, 1094, 1010, 941, 933, 843, 803, 769, 742, 729.

2-(4-Bromophenyl)-6-methylimidazo [1,2-a] pyridine (4)

^{1}H NMR: δ 8.77 (d, J = 0.7 Hz, 1H), 8.68 (q, J = 1.3 Hz, 1H), 8.00 – 7.93 (m, 2H), 7.85 (d, J = 9.1 Hz, 1H), 7.80 – 7.73 (m, 3H), 2.40 (d, J = 1.2 Hz, 3H). ^{13}C NMR: δ 146.35 , 139.60 , 136.25 , 134.95 , 132.77 , 128.55 , 127.46 , 126.88 , 126.49 , 123.97 , 111.92 , 111.62 , 17.87 . HRMS (ESI) calculated m/z, 287.0178; found $C_{14}H_{12}BrN_2$ m/z, 287.0178 $[M + H]^+$. IR (cm^{-1}): 2534, 2364, 2161, 2023, 1978, 1655, 1525, 1488, 1455, 1443, 1274, 1067, 1007, 839, 804, 786, 774, 742, 712.

6-Methyl-2-(4-nitrophenyl) imidazo [1,2-a] pyridine (5)

^{1}H NMR: δ 8.79 (s, 1H), 8.58 (d, J = 1.6 Hz, 1H), 8.42 – 8.28 (m, 2H), 8.34 – 8.18 (m, 2H), 7.76 (d, J = 9.2 Hz, 1H), 7.59 (d, J = 9.3 Hz, 1H), 2.36 (d, J = 1.1 Hz, 3H). ^{13}C NMR: δ 147.77 , 141.60 , 134.34 , 127.31 , 126.33 , 126.01 , 124.81 , 113.68 , 112.96 , 109.99 , 56.45 , 19.00 , 17.89 . HRMS (ESI) calculated m/z, 254.0924; found $C_{14}H_{11}N_3O_2$ m/z, 254.0924 $[M + H]^+$. IR (cm^{-1}): 2521, 2364, 2160, 2022, 1977, 1601, 1509, 1490, 1449, 1343, 1264, 1245, 1221, 1108, 854, 834, 806, 768, 752, 741, 715.

2-(4-methoxyphenyl)-6-methylimidazo [1,2-a] pyridine (6)

^{1}H NMR: δ 8.67 (q, J = 1.2 Hz, 1H), 8.63 (d, J = 0.7 Hz, 1H), 8.03 – 7.97 (m, 2H), 7.86 (d, J = 9.1 Hz, 1H), 7.77 (dd, J = 9.2, 1.6 Hz, 1H), 7.15 – 7.09 (m, 2H), 3.83 (s, 2H), 2.50 (p, J = 1.8 Hz, 3H), 2.41 (d, J = 1.1 Hz, 2H). ^{13}C NMR: δ 161.2, 139.1, 135.8, 135.8, 128.3, 127.4, 126.7, 119.2, 115.2, 111.6, 109.9, 55.9, 17.9. HRMS (ESI) calculated m/z, 239.1179; found $C_{15}H_{15}N_2O$ m/z, 239.1179 $[M + H]^+$. IR (cm^{-1}): 2539, 2436, 2366, 2157, 2028, 1975, 1660, 1617, 1594, 1577, 1561, 1507, 1441, 1367, 1294, 1256, 1186, 1160, 1023, 952, 840, 808, 795, 743.

4-(6-methylimidazo [1,2-a] pyridin-2-yl) phenol (7)

^{1}H NMR: δ 10.22 (s, 1H), 8.66 (s, 1H), 8.54 (s, 1H), 7.85 (dd, J = 9.0, 2.3 Hz, 3H), 7.76 (dd, J = 9.2, 1.5 Hz, 1H), 7.03 – 6.90 (m, 2H), 2.41 (d, J = 1.2 Hz, 3H). ^{13}C NMR δ 159.7, 139.5, 137.2, 134.9, 128.2, 126.8, 126.5, 118.3, 116.5, 112.0, 109.2, 17.9. HRMS (ESI) calculated m/z, 225.1022; found $C_{14}H_{15}N_2O$ m/z, 225.1022 $[M + H]^+$. IR (cm^{-1}): 2489, 2158, 2027, 1975, 1617, 1591, 1506, 1459, 1397, 1375, 1292, 1275, 1246, 1219, 1179, 1112, 951, 837, 812, 766, 741.

4-(6-methylimidazo [1,2-a] pyridin-2-yl) benzonitrile (8)

^{1}H NMR: δ 8.90 (s, 1H), 8.70 (q, J = 1.3 Hz, 1H), 8.29 – 8.18 (m, 2H), 8.09 – 7.98 (m, 2H), 7.88 (d, J = 9.2 Hz, 1H), 7.79 (dd, J = 9.3, 1.5 Hz, 1H), 2.41 (d, J = 1.1 Hz, 3H). ^{13}C NMR: δ 140.1, 136.4, 134.5, 133.6, 131.9, 127.4, 127.2, 126.9, 118.8, 113.0, 112.5, 112.2, 17.9. HRMS (ESI) calculated m/z, 234.1026; found $C_{15}H_{12}N_3$ m/z, 234.1026 $[M + H]^+$. IR (cm^{-1}): 2781, 2702, 2536, 2498, 2446, 2368, 2156, 2025, 1974, 1656, 1613, 1557, 1528, 1498, 1446, 1302, 1267, 1163, 1135, 1039, 1021, 996, 950, 8757, 848, 835, 808, 791, 746, 717.

6-methyl-2-(3-nitrophenyl) imidazo [1,2-a] pyridine (9)

^{1}H NMR: δ 8.79 (t, J = 2.0 Hz, 1H), 8.68 (s, 1H), 8.47 (q, J = 1.4 Hz, 1H), 8.42 (dt, J = 7.8, 1.3 Hz, 1H), 8.21 (dd, J = 8.2, 1.0 Hz, 1H), 7.78 (t, J = 8.0 Hz, 1H), 7.66 (d, J = 9.2 Hz, 1H), 7.38 (dd, J = 9.0, 1.7 Hz, 1H), 2.34 (s, 3H). ^{13}C NMR: δ 150.31, 142.50, 137.70, 136.28, 133.14, 131.96, 131.58, 128.54, 127.49, 125.29, 121.80, 113.70, 113.01, 18.10.. HRMS (ESI) calculated m/z, 254.0924; found $C_{14}H_{12}N_3O_2$ m/z, 254.0924 $[M + H]^+$. IR (cm^{-1}): 2947, 2930, 2541, 2456, 2363, 2158, 2028, 1974, 1656, 1619, 1554, 1517, 1486, 1456, 1348, 1266, 1215, 1163, 1114, 1071, 970, 904, 879, 837, 808, 768, 724.

6-methyl-2-(2-nitrophenyl) imidazo [1,2-a] pyridine (10)

^{1}H NMR: δ 8.40 – 8.34 (m, 1H), 8.18 (d, J = 0.7 Hz, 1H), 7.91 (dd, J = 7.8, 1.4 Hz, 1H), 7.83 (dd, J = 8.0, 1.2 Hz, 1H), 7.71 (td, J = 7.6, 1.3 Hz, 1H), 7.56 (td, J = 7.7, 1.4 Hz, 1H), 7.48 (d, J = 9.1 Hz, 1H), 7.14 (dd, J = 9.2, 1.7 Hz, 1H), 2.28 (d, J = 1.1 Hz, 3H). ^{13}C NMR: δ 149.2, 144.1, 140.0, 132.4, 130.9, 129.2, 129.0, 127.4, 124.9, 124.0, 122.3, 116.7, 111.1, 18.0. HRMS (ESI) calculated m/z, 254.0924; found $C_{14}H_{12}N_3O_2$ m/z, 254.0924 $[M + H]^+$. IR (cm^{-1}): 2540, 2487, 2443, 2364, 2341, 2159, 2027, 1974, 1609, 1527, 1459, 1420, 1372, 1345, 1285, 1260, 1208, 1164, 1144, 1105, 1033, 1018, 990, 949, 854, 836, 800, 776, 761, 727.

2-(3-fluorophenyl)-6-methylimidazo [1,2-a] pyridine (11)

^{1}H NMR: δ 8.83 (s, 1H), 8.71 (q, J = 1.2 Hz, 1H), 7.97 (dt, J = 10.2, 2.2 Hz, 1H), 7.96 – 7.83 (m, 2H), 7.81 (dd, J = 9.2, 1.5 Hz, 1H), 7.62 (td, J = 8.1, 6.0 Hz, 1H), 7.43 – 7.28 (m, 1H), 2.41 (d, J = 1.1 Hz, 3H). ^{13}C NMR: δ 162.9 (d, J = 244.2 Hz), 139.6 , 136.4 , 134.7 (d, J = 2.8 Hz), 132.0 (d, J = 8.5 Hz), 129.4 (d, J = 8.8 Hz), 127.5 , 126.9 , 122.8 (d, J = 2.9 Hz), 117.4 (d, J = 21.1 Hz), 113.5 (d, J = 24.1 Hz), 112.0 , 111.9 , 17.8 . HRMS (ESI) calculated m/z, 227.0979; found $C_{14}H_{11}FN_2$ m/z, 227.0979 $[M + H]^+$. IR (cm^{-1}): 3058, 3023, 3012, 2929, 2536, 2448, 2366, 2157, 2102, 2024, 1975, 1664, 1604, 1585, 1529, 1491, 1452, 1362, 1311, 1271, 1196, 1159, 1088, 799, 879, 816, 795, 746.

2-(2-fluorophenyl)-6-methylimidazo[1,2-a] pyridine (12)

^{1}H NMR: δ 8.75 (q, J = 1.3 Hz, 1H), 8.64 (d, J = 3.0 Hz, 1H), 8.26 (td, J = 7.8, 1.7 Hz, 1H), 7.91 (d, J = 9.2 Hz, 1H), 7.81 (dd, J = 9.2, 1.6 Hz, 1H), 7.63 – 7.53 (m, 1H), 7.53 – 7.41 (m, 2H), 2.41 (s, 3H). ^{13}C NMR: δ 159.6 (d, J = 250.8 Hz), 139.4 , 136.3 , 132.5 (d, J = 9.0 Hz), 130.0 , 128.9 , 127.2 , 126.8 , 125.9 , 117.0 (d, J = 21.4 Hz), 115.5 (d, J = 11.9 Hz), 113.8 (d, J = 14.0 Hz), 112.0 , 18.0 (d, J = 3.7 Hz). HRMS (ESI) calculated m/z, 227.0979; found

$C_{15}H_{14}FN_2$ m/z, 227.0979 $[M + H]^+$. IR (cm^{-1}): 2930, 2542, 2449, 2371, 2160, 2025, 1973, 1656, 1621, 1523, 1498, 1451, 1357, 1313, 1268, 1227, 1164, 1118, 949, 861, 805, 764, 743.

Data and Software Availability

All DNA microarray data have been deposited in GEO under the accession number: GSE123668. RNA-Sequencing data have been deposited in the Bioproject database, NCBI. The accession number is SUB4899089.

SUPPLEMENTAL REFERENCES

Ashburner, M., Ball, C.A., Blake, J.A., Botstein, D., Butler, H., Cherry, J.M., Davis, A.P., Dolinski, K., Dwight, S.S., Eppig, J.T., *et al.* (2000). Gene ontology: tool for the unification of biology. The Gene Ontology Consortium. Nat Genet *25*, 25-29.

Benjamini, Y., and Hochberg, Y. (1995). Controlling the False Discovery Rate: A Practical and Powerful Approach to Multiple Testing. Journal of the Royal Statistical Society Series B (Methodological) *57*, 289-300.

Cheng, X., Dimou, E., Alborzinia, H., Wenke, F., Gohring, A., Reuter, S., Mah, N., Fuchs, H., Andrade-Navarro, M.A., Adjaye, J., *et al.* (2015a). Identification of 2-[4-[(4-Methoxyphenyl)methoxy]-phenyl]acetonitrile and Derivatives as Potent Oct3/4 Inducers. J Med Chem *58*, 4976-4983.

Cheng, X., Merz, K.H., Vatter, S., Zeller, J., Muehlbeyer, S., Thommet, A., Christ, J., Wolfl, S., and Eisenbrand, G. (2017). Identification of a Water-Soluble Indirubin Derivative as Potent Inhibitor of Insulin-like Growth Factor 1 Receptor through Structural Modification of the Parent Natural Molecule. J Med Chem *60*, 4949-4962.

Cheng, X., Yoshida, H., Raoofi, D., Saleh, S., Alborzinia, H., Wenke, F., Gohring, A., Reuter, S., Mah, N., Fuchs, H., *et al.* (2015b). Ethyl 2-((4-Chlorophenyl)amino)thiazole-4-carboxylate and Derivatives Are Potent Inducers of Oct3/4. J Med Chem *58*, 5742-5750.

Dunning, M.J., Smith, M.L., Ritchie, M.E., and Tavare, S. (2007). beadarray: R classes and methods for Illumina bead-based data. Bioinformatics *23*, 2183-2184.

Gentleman, R.C., Carey, V.J., Bates, D.M., Bolstad, B., Dettling, M., Dudoit, S., Ellis, B., Gautier, L., Ge, Y., Gentry, J., *et al.* (2004). Bioconductor: open software development for computational biology and bioinformatics. Genome Biology *5*, R80.

Onder, T.T., Kara, N., Cherry, A., Sinha, A.U., Zhu, N., Bernt, K.M., Cahan, P., Marcarci, B.O., Unternaehrer, J., Gupta, P.B., *et al.* (2012). Chromatin-modifying enzymes as modulators of reprogramming. Nature *483*, 598-602.

Szklarczyk, D., Santos, A., von Mering, C., Jensen, L.J., Bork, P., and Kuhn, M. (2016). STITCH 5: augmenting protein-chemical interaction networks with tissue and affinity data. Nucleic acids research *44*, D380-384.

Takahashi, K., Tanabe, K., Ohnuki, M., Narita, M., Sasaki, A., Yamamoto, M., Nakamura, M., Sutou, K., Osafune, K., and Yamanaka, S. (2014). Induction of pluripotency in human somatic cells via a transient state resembling primitive streak-like mesendoderm. Nat Commun *5*, 3678.

Vassena, R., Boue, S., Gonzalez-Roca, E., Aran, B., Auer, H., Veiga, A., and Izpisua Belmonte, J.C. (2011). Waves of early transcriptional activation and pluripotency program initiation during human preimplantation development. Development *138*, 3699-3709.